Review

Johann Toudert*

Spectroscopic ellipsometry for active nano- and meta-materials

Abstract: Spectroscopic ellipsometry (SE) is a powerful technique for the characterization of materials, which is able to probe in a sensitive way their nanostructure as well as to get rich information about their dielectric properties, through the interaction of polarized light with matter. In the present trend of developing functional advanced materials of increasing complexity for a wide range of technological applications, works involving SE have flourished and have been reported in an increasing number of articles, reviews, and books. In this context, the aim of this paper is to provide for those among material scientists who are not SE specialists, a concise and updated overview of the capabilities of SE for the characterization of the so-called nano- and metamaterials, especially those presenting active functionalities. Key aspects for a reliable material characterization by SE are given: choice of the setup and measurement conditions, measurement accuracy, definition of a model, sensitivity to parameters. Also, very recent works involving SE are highlighted, especially those dealing with the development of building block materials for optimized or active plasmonics applications, the still ongoing exploration of small-size effects on the dielectric response of matter, the characterization of metamaterials, and the design of detectors with improved accuracy based on coupling of the phase sensitivity of SE with metamaterials engineering.

Keywords: active plasmonics; metamaterials; nanostructured materials; sensing; spectroscopic ellipsometry.

***Corresponding author: Johann Toudert,** Laser Processing Group, Nanoscience and Photonics Division, Instituto de Óptica – CSIC, Serrano 121, Madrid, Spain, e-mail: johann.toudert@gmail.com

1 Introduction

Since the first experiments involving polarized light in the 19th century [1], advances in the field of instrumentation, data acquisition, and analysis have allowed the development of the spectroscopic ellipsometry (SE) technique as it is known today. Many books and reviews (such as those of Azzam and Bashara [2], Tompkins and Irene [3], Fujiwara [4]), Losurdo et al. [5], Oates et al. [6], Losurdo and Hingerl [7]) are devoted to SE and its applications. In this context of plenty of already published material, the aim of this article is to provide for those among material scientists who are not SE specialists, a concise and updated overview of the capabilities of SE. Also, it highlights very recent works involving this technique for the characterization of nano- or metamaterials, whose interaction with electromagnetic waves would be sensitive to external physical parameters such as temperature, chemical environment, etc. Such so-called active materials are of important interest in many fields of applied physics, such as, optical data recording, switching, smart window design, or sensing. A special emphasis will be made on materials for active plasmonics, as they are at the focus of very trendy research topics [8, 9]. Also, a critical discussion on the use of SE for the exploration of small-size effects on the dielectric function of matter will be proposed.

SE is based on the measurement of changes in the polarization of electromagnetic waves upon interaction with the probed material. Standard SE measurements involve an incident beam of linearly polarized radiation, usually described in terms of its s and p components (perpendicular and parallel to the plane of incidence, respectively) (see Figure 1A). The amplitude and phase of these two components are changed upon reflection, possibly in a different way. Consequently, the (specularly) reflected beam may present an elliptic polarization state, which is to be analyzed (thus, the term “ellipsometry” – note that ellipsometry can also be performed with transmitted light; this case will not be considered in the present article). In the simplest case of a compositionally homogeneous (i.e., monophase, nonporous) semi-infinite material with isotropic dielectric properties and a perfectly flat interface with the external medium (usually air), an incident s-polarized (p-polarized) beam remains s-polarized (p-polarized) upon reflection. The interaction of the

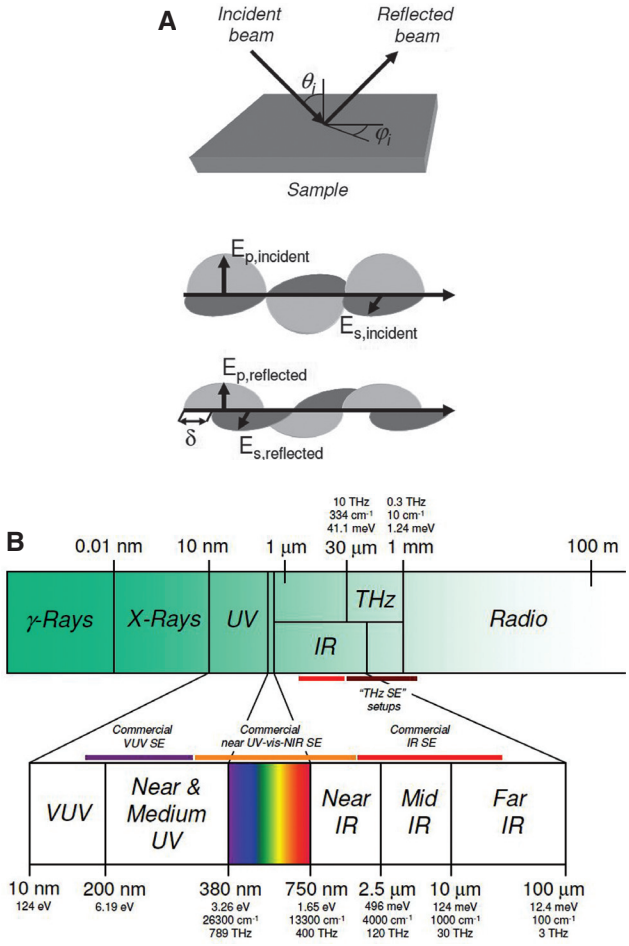

Figure 1 Ellipsometry and its spectral range. (A) Schematic representation of a typical spectroscopic ellipsometry configuration (in reflection); the angle of incidence θ_i and azimuth φ_i are depicted, as well as the phase shift δ between the s- and p-components of the electromagnetic wave induced by reflection on the substrate. The plane of incidence is the plane of the paper (B). Schematic representation of the electromagnetic spectrum, together with the typical spectral ranges accessible using the different types of spectroscopic ellipsometry setups.

probe beam with this material is thus fully described by the complex Fresnel reflection coefficients, r_p and r_s. r_p (r_s) links the amplitude and phase of the p-polarized (s-polarized) reflected wave to those of the incident p-polarized (s-polarized) wave. The measured quantity is usually the ratio r_p/r_s, which is generally expressed as a function of Ψ and Δ that carry the amplitude and phase information, respectively. These two so-called ellipsometric angles are analytically related to the real (ε_1) and imaginary (ε_2) part of the material's dielectric function ε (or in other words, to its refractive index n and extinction coefficient k), which can therefore be determined from a single ellipsometry measurement at oblique incidence. As measurements are usually performed at several wavelengths in vacuum λ_0 (or energies E), thus permitting to obtain $\varepsilon(\lambda_0)$ (or ε(E)), ellipsometry is denoted as "spectroscopic."

Nowadays, SE measurements can be performed from the vacuum ultraviolet (VUV) to the THz. Evaluation of the dielectric function of a material in such a broad spectral range allows to probe its electronic structure as well as vibrational modes. Besides, although most SE measurements involve macroscopic beams, ellipsometric imaging with microscale resolution can be performed on several setups, and proof-of-concept of nanoscale ellipsometric imaging has been reported. The potential of SE for covering a broad spectral range and allowing measurements with a fine spatial in-plane resolution is evoked in Section 2.

As materials are generally not homogeneous, isotropic, and semi-infinite with a perfectly flat interface with the exterior medium, SE can be used for getting information about the heterogeneity, anisotropy, roughness, and thickness of the probed material. However, a reliable extraction of such information requires adequate SE setup and measurement conditions to be chosen and a sufficient measurement accuracy to be achieved. In addition, this information can generally not be determined directly from the measurement but requires to model and fit the data and to evaluate the sensitivity of the measured data to the parameters to be extracted. For these reasons, SE is a setup-dependent and model-dependent technique, requiring the user to be sufficiently trained, both from the experimental and theoretical points of views. These aspects are highlighted in Section 3.

As said above, although materials can be fabricated to behave as semi-infinite (or bulk) in regard to the incoming waves (no radiation reaches their back face), in many cases, they are produced as thin films in which back reflections of waves may come into play. There are plenty of published works devoted to the SE characterization of materials under the form of bulk or thin films. In Section 4, very recent works that deal with SE as a monitoring tool for the optimization of bulk or thin film building block materials (metals, metal-based nitrides) aiming at plasmonic applications will be highlighted. Then, the importance of SE in the characterization of building block materials for active plasmonics (electrochromic materials, phase-transition materials) will be highlighted.

Section 5 is devoted to ultrathin films, which represent the limit of thin films in the low thickness (of a few nm) regime. Two cases will be distinguished: i) continuous films presenting dielectric properties different from those of their bulk or thicker counterparts due to confinement effects; ii) granular films, consisting of separated nanostructures (NSs), which thus present effective dielectric

properties driven by the size, morphology, organization of the NSs, and their individual dielectric response.

It is well known that the individual dielectric response of NSs can be different from that of their bulk counterpart, due to small-size induced effects. The determination of the dielectric function of NSs, such as nanoparticles (NPs), nevertheless, remains an open field of research. Section 6 thus highlights recent SE works aiming at the determination of the dielectric function of Si NPs embedded in transparent thin film matrices. It is highlighted that efforts for the development of tailor-made materials and proper theoretical modeling are still needed for a reliable and accurate extraction of the response of semiconductor or metal NPs from macroscopic measurements on such composite media.

Section 7 deals with recent successful attempts of SE characterization on metamaterials. Such materials are designed artificially by arranging nanoscale building blocks, in order to generate original effects such as birefringence or dichroism, optical magnetism, or negative refraction. However, their characterization by SE is a quite complex task that requires adequate measurements and modeling. SE measurements are nondestructive, noncontact, and can be realized *in situ*, thus permitting to track the evolution of the material's response as a function of externally tuned parameters, such as temperature, magnetic field, chemical environment. Also, they are generally self-referenced (i.e., no reference measurement of the radiation source intensity is required), thus allowing to perform intensity fluctuation-free measurements. Last but not the least, as they carry phase information, they allow a particular accuracy that has sustained the development of SE-based surface plasmon resonance sensors. Recently, and as explained in Section 7, coupling SE with plasmonic metamaterials has opened the way to the development of ultrasensitive nanostructured detectors.

2 From the vacuum ultraviolet to the terahertz, toward nanoscale ellipsometric imaging

2.1 Wide spectral range accessible by spectroscopic ellipsometry measurements

SE is used as a measurement tool in the near-ultraviolet (UV) to near-infrared (IR) range for the characterization of a broad range of materials. Measurements in the vacuum UV [10, 11] and in a broad spectral range in the IR [12–15] have also been made possible either using "home-built" or commercial setups. More recently and although still being in its infancy, THz SE [16, 17] has already provided promising results. Performing measurements of a material's dielectric function ε (assuming the most simple case of a compositionally homogeneous and isotropic medium) in such a broad spectral range from the vacuum UV to the THz (see Figure 1B) yields rich information about the material's electronic structure. For instance, measurements in the vacuum UV are suitable for probing the band-gap region of wide band-gap semiconductors; interband transitions in metals can be observed in the UV, visible, or IR depending on the material, whereas the contribution of free charge carriers, if sizeable in the visible for metals like Ag or Au, must be sought further toward the THz in materials presenting extremely low free-charge carrier densities. Besides, phonons can also be revealed [4, 12, 18] in the IR, as well as their coupling with electronic excitations (for instance, phonon-plasmon coupling [18]). Many more excitations can be probed, such as polarons [12] and plasmarons [19].

2.2 Imaging ellipsometry: down to a nanoscale resolution

In addition to its use for extracting spectral information, SE gives access to the value of nanoscale parameters, such as the thickness of thin films, possibly with a precision at the ångström level or the dimension of nanostructures. These values are traditionally obtained from measurements performed with macroscopic beams and require adequate data modeling, as it will be detailed in the following sections. Besides, efforts have been made in order to reduce the beam dimensions so that a precise imaging of the samples could be realized. Spot sizes in the visible can now be reduced from a few millimeters to less than 100 of micrometers. In that way, ellipsometric micro-imaging has been achieved. Moreover, a few demonstrations of ellipsometry measurements with subwavelength lateral resolution have been reported [20, 21]. In the so-called near-field ellipsometry setups, transparent films presenting a rough surface, containing near-surface embedded NPs, or consisting of a multiphase material are illuminated through a transparent substrate, in a total internal reflection configuration [20] or traditional [21] configuration. An atomic force microscopy metal coated tip is scanned over the film surface, and the perturbation of the ellipsometric signal due to tip-induced scattering of light with modified polarization is recorded as a function of the tip location.

3 Key aspects for a reliable spectroscopic ellipsometry analysis: setup, measurement conditions and accuracy, modeling, sensitivity to parameters

SE is suitable for providing much more information than the dielectric function of homogeneous isotropic bulk materials. In fact, it can be employed for the characterization of a wide range of materials, ranging from isotropic homogeneous thin films to complex metamaterials displaying biaxial effective anisotropy, optical magnetism, or chirality. Such characterization, however, requires to choose adequately the SE setup and measurement conditions, as well as to fit simulated data to the measured ones using meaningful models or numerical methods. In the following subsections, insights into these aspects are given for different kinds of samples.

3.1 Standard SE: materials with diagonal Jones matrix

Near UV-to-near IR SE measurements are routinely performed on flat, isotropic, and homogeneous thin films deposited on an opaque, flat, isotropic, and homogeneous substrate in order to evaluate their thickness and dielectric function ε. The overall response of this kind of sample is described at each wavelength by a 2*2 Jones matrix that links the complex s-polarized and p-polarized components of the reflected electric field to those of the incident field. This matrix is diagonal with elements r_p and r_s; i.e., a purely s-polarized (p-polarized) incident wave remains s-polarized (p-polarized) after reflection. As explained in Section 1, standard SE measurements allow to determine the wavelength-dependent ratio $\rho=r_p/r_s$ between the diagonal elements of the Jones matrix, usually represented by the ellipsometric angles Δ and Ψ. The determination scheme of these two angles is based on measurements of the reflected intensity for several orientations of polarizing elements (in the plane of polarization) placed before and after the sample. More details about the Δ and Ψ determination scheme are given in ref. [4] in relation with many available SE setups. The spectral measurements are usually performed at several angles of incidence θ_i (see Figure 1A) in order to increase the ratio between the number of experimental data and the number of parameters to be evaluated at each wavelength. This evaluation is based on the fitting of simulated Δ and Ψ spectra (or of the related r_p/r_s ratio) to the measured ones. Calculation of these spectra is performed during the fitting procedure through the derivation of the wavelength-dependent Jones matrix of the sample in the 2*2 Abelès multilayer matrix formalism, using the film thickness and dielectric function as adjustable parameters, the substrate dielectric function being fixed at his known value. Spectral fitting can be performed wavelength-by-wavelength or using a physically meaningful mathematical model for the wavelength dependence of ε, thus, potentially reducing the number of parameters and possibly imposing Kramers-Krönig consistency for ε. The same procedure can be applied to multilayer thin films based on flat, isotropic, and homogeneous layers or to homogeneous uniaxial anisotropic layers (whose dielectric response is described by a tensor, $[\varepsilon]$) with their optical axis perpendicular to the sample surface (see refs. [2–4] for more details).

3.2 Generalized SE: materials with nondiagonal Jones matrix

Uniaxial anisotropic materials (bulk or thin layers with flat interfaces) with their optical axis tilted from the sample's normal are described at each wavelength by a nondiagonal Jones matrix, whose extradiagonal terms, r_{ps} and r_{sp}, account for p-to-s and s-to-p polarization conversion. Generalized SE measurements consist in the determination of these extradiagonal terms in addition to the diagonal ones denoted as r_{pp} and r_{ss}, usually through the measurement of six independent parameters: Ψ_{pp} and Δ_{pp}, Ψ_{ps} and Δ_{ps}, Ψ_{sp} and Δ_{sp}. These parameters account for the amplitude and phase of the $\rho_{pp}=r_{pp}/r_{ss}$, $\rho_{ps}=r_{ps}/r_{ss}$, and $\rho_{sp}=r_{sp}/r_{ss}$ ratios, respectively. In order to determine the values of these parameters at a given wavelength, measurements are usually performed at several angles of incidence θ_i and azimuths φ_i (see Figure 1A). Calculations of the Jones matrix during the fitting procedure are done using the 4*4 Berreman multilayer matrix formalism [4, 22, 23], using the layers' thickness and dielectric tensor as adjustable parameters. Such approach is also valid for biaxial materials. SE on materials with nondiagonal Jones matrix is referred as "generalized" [2]. Note that anisotropy can be intrinsic to the material or induced by an external excitation. For instance, when an isotropic conducting material (initially described by a dielectric function ε) is placed in a constant magnetic field, its dielectric response can be turned anisotropic (i.e., it is described by a tensor $[\varepsilon]$). This is known as the "optical Hall effect" [24, 25]. Measuring the magnetic field-induced dielectric anisotropy of the material allows a noncontact determination

of the free-carrier effective mass and (in principle) type [18, 24].

3.3 Effective medium modeling of rough interfaces and nanostructured media

Up to now, only bulk homogeneous materials with smooth surfaces and thin films with flat interfaces have been evoked. However, materials presenting rough interfaces, or containing NSs such as NPs or nanorods, are frequently encountered. Provided the characteristic dimensions of such heterogeneities can be neglected *versus* the wavelength of the probing radiation, the effective medium approximation is usually made [4, 6, 26]. For instance, a (weakly) rough interface or a NPs:matrix composite film are often considered as an equivalent homogeneous thin layer with an effective dielectric function ε_{eff} or tensor $[\varepsilon_{eff}]$. Fitting to the measured spectra (still involving the Abelès or Berreman multilayer approaches) gives access to the effective dielectric response of the layer, from which nanostructural information can be extracted provided an adequate effective medium model is used.

3.4 Depolarization and Mueller matrix SE

Surface/interface roughness or other heterogeneities at the wavelength scale [27], thickness inhomogeneity [28], detection of radiation reflected (incoherently) from the backside of a thick transparent substrate [27, 29], noncollimated beam, may induce depolarization of the measured reflected beam. Depolarizing samples cannot be described in the Jones formalism; instead, they require the measurement of, at least, part of the (real) 4*4 Mueller matrix that links the Stokes vector of the reflected beam to that of the incident beam [4]. In the Stokes formalism, the polarization state of light is decomposed on the basis of linearly and circularly polarized components in the plane of polarization: four linearly polarized components along the x and y axes and tilted at +45° and -45° from these axes and two circularly polarized components with a right and left rotation. The four elements S_i of the Stokes vector of a beam are obtained from the intensities of its linearly and circularly polarized components, following: $S_0=I_x+I_y$, $S_1=I_x-I_y$, $S_2=I_{+45}-I_{-45}$, and $S_3=I_R-I_L$. The Stokes vector is suitable for the description of fully polarized light or partially polarized light. In the latter case, the degree d of polarization is given by $s=(S_1^2+S_2^2+S_3^2)^{1/2}/S_0$. Therefore, using Mueller matrix SE, depolarization can be measured and seen as additional information about the sample (note that Mueller matrix SE, as a more general measurement route than the Jones formalism-based SE, is of course suitable to the case of less-complex nondepolarizing samples). Nevertheless, the simultaneous presence of roughness with other depolarization sources may induce a loss of depolarization information [27], in case of significant roughness-induced diffuse scattering of the electromagnetic radiation (which is not collected by the detector in usual SE measurements that involve a specular/θ-2θ geometry). A more complete characterization of samples presenting diffuse scattering requires performing scatterometry measurements.

3.5 Optically magnetic and chiral metamaterials

The development of nanofabrication techniques in the last decades have permitted to design artificial materials (among the so-called metamaterials [30]) based on 2D arrays of sub-wavelength scale structures whose interaction with electromagnetic radiation involves cross-coupling between electric/electric displacement and magnetic/magnetic induction fields [31]. In this case, if the material can be considered as an effective medium, its electromagnetic properties shall be described by several tensors: dielectric permittivity $[\varepsilon_{eff}]$, magnetic permeability $[\mu_{eff}]$, chirality $[\gamma_{eff}]$ and $[\zeta_{eff}]$, which have to be retrieved from fitting of the measured SE data (using the Berreman multilayer matrix formalism). Also, it has been suggested that Mueller matrix SE on an effective medium material displaying optical magnetism (i.e., with a nonzero magnetic permeability tensor) is required for separating the magnetic and dielectric contributions to its effective response and recording necessary information for evidencing negative refraction [32]. Note that the effective medium description of metamaterials (and of rough surfaces) is not always legitimate, as evoked in Section 7. In such a case, meaningful fitting of the measured data requires going beyond the multilayer matrix formalisms cited above. In this context, numerical calculations (such as finite difference time domain or rigorous coupled-wave approximation) that take into account accurately the material's structure become necessary tools.

3.6 Choosing an adequate setup and measurement conditions, using meaningful models

Many commercial and "home-built" SE setups exist, whose configuration dictates the type of measurements

that can be performed (spectral and angular range, measurement of the Jones matrix or Mueller matrix, acquisition time and implementation for *in situ* experiments, imaging capability). For a detailed description of the capabilities of the different ellipsometry setups, see ref. [4]. Much can already be done with a desktop near UV-to-near IR Polarizer-Sample-Rotating Analyzer spectroscopic ellipsometer (almost the simplest setup), which allows generalized SE measurements [22]. At the other extremity, ultrafast real-time measurements of the complete Mueller matrix in the visible can be done using a multichannel Polarizer-rotating Compensator Sample-rotating Compensator-Analyzer setup [33]. Therefore, the setup must be chosen according to the type of sample and properties to be characterized. Also, the choice of measurement conditions (angle and medium of incidence, azimuth, substrate, spectral range) is important as sensitivity of the SE measurement to a given unknown parameter may be weak or even zero in some conditions and strong in others. As a first simple example, the thickness of a thin film cannot be determined in a spectral region where it is absorbing enough so that electromagnetic waves do not reach the interface with the substrate (thicknesses superior to 1000 nm in Figure 2A). As a second example, standard SE measurements on a uniaxial non-absorbing bulk material with its optical axis perpendicular to the (flat) surface present a relatively low sensitivity to the material's extraordinary refractive index n_e. Figure 2B shows the evolution of Ψ as a function of the angle of incidence θ_i for different values of n_e, the ordinary refractive index n_o being fixed at 1.8. An index contrast $\Delta n=n_o-n_e=0.1$ leads to a variation of the Brewster angle θ_B and Ψ of around 1° when compared to the isotropic case ($\Delta n=0$). The precision limit for θ and Ψ measurements on current commercial measurements is in the range of 0.01°, thus allowing the detection of a very weak anisotropy. Nevertheless, it is worth noting that, the lower the index contrast, the higher must be the accuracy of the ellipsometer calibration, alignment, and the lower the noise level, so that the Δn value could be determined in a reliable way. Alternatively, in the case of uniaxial bulk non-absorbing crystals, the sensitivity to the extraordinary refractive index can be enhanced by realizing generalized SE measurements on a cleaved crystal, so that its optical axis is tilted away from the normal to the surface [22]. For absorbing uniaxial thin films, increasing the sensitivity to the out-of-plane dielectric function can be done upon coupling and extracting the polarized light through a prism [34].

Third, in the case where the values of several parameters are unknown, their precise determination may be complicated due to correlation between them, as it is the case for ultrathin transparent films, for which several combinations of thickness and refractive index may yield reasonable fits of the experimental data [35]. Indeed, as shown in Figure 2C, Ψ and Δ spectra presenting similar structures are obtained with two couples of (n,t) values (n=1.8, t=2.5 nm; n=1.25, t=5 nm) for a transparent ultrathin film deposited on a Si substrate. Nevertheless, as seen in the inset of the same figure, the two (n,t) couples yield a significantly different ellipsometric response in

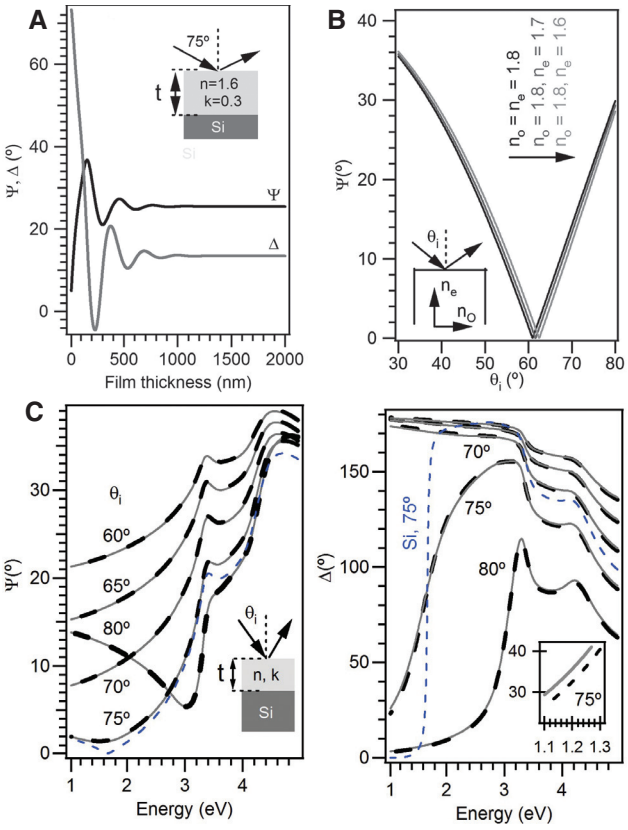

Figure 2 Some examples of spectroscopic ellipsometry analysis – parameter sensitivity and correlation between parameters. (A) Ellipsometric angles *versus* the thickness t of a thin film (n=1.6, k=0.3) on a Si substrate, at an incident angle θ_i=75° and a wavelength in vacuum λ_0 of 800 nm. (B) Ψ *versus* θ_i for an isotropic crystal (n=1.8, k=0, black curve), a uniaxial crystal with its optical axis normal to the surface (n_o=1.8, n_e=1.7, k=0 – brown curve; n_o=1.8, n_e=1.6, k=0 – orange curve). The Ψ difference between the uniaxial and isotropic crystals is less than 1° for an index contrast n_o-n_e of 0.1. (C) Spectra of the ellipsometric angles of an ultrathin film on Si for different values of θ_i, with n=1.8, k=0 and t=2.5 nm (dashed line) and with n=1.218, k=0 and t=5 nm. The curves present similar structures thus evidencing the n-t parameter correlation. Nevertheless, for well-chosen angle of incidence and spectral range, significant differences between the two curves can be seen, as shown in the inset that displays the Δ spectra at θ_i=75° in the 1.1 eV–1.3 eV range. Also shown are spectra of bare bulk Si, in order to evidence the strong sensitivity of Δ to the presence of a transparent ultrathin film.

some spectral regions and at specific angles of incidence. Therefore, in order to determine the values of (n,t), the prior task consists of searching for measurement conditions for which the coupling between the parameters is minimized. In addition, it is necessary to evaluate the sensitivity of the ellipsometric spectra to the different parameters, which has to be compared with the measurement accuracy. In the case where the variation of a given parameter does not induce changes in the ellipsometric spectra above the measurement error, its evaluation makes no sense. In this context, modern commercial ellipsometry analysis/fitting software allow to realize parameter-sensitivity or parameter-correlation tests that can be of great help for choosing suitable measurement conditions and performing a reliable data analysis. Nevertheless, as the first task of such analysis is the definition of a model for the studied sample, the training and critical mind of the user are primordial for obtaining meaningful results. The user must be aware of the fundamental aspects of ellipsometry and of physical criteria so that he can decide if mathematically correct solutions are reliable or not. Also, note that usual commercial ellipsometry analysis software is based on multilayer matrix calculations and effective medium approximations. Therefore, in the case of materials for which it is not legitimate to use these theoretical formalisms, external simulation codes have to be used. Also, depending on the complexity of the problem, the user may also decide to characterize the samples using other techniques in order to determine the value of some unknown parameters.

4 Determining the dielectric function of bulk- or thin film- building block materials for optimized or active plasmonic devices

The development of plasmonic devices requires to elaborate tailor-made NSs (NPs, nanorods, nanostripes, thin films, perforated thin films) whose plasmonic behavior can be tuned through the control of their size, morphology, or organization. Nevertheless, the tunability range of plasmonic effects is defined by the dielectric function of the material ε the NSs are built from. Therefore, choosing a suitable building block material for the NSs is the first issue that has to be tackled prior to the development of a plasmonic device. During a long time, plasmonics has been mostly related with Ag and Au and consequently mainly limited to the near UV-to-near IR spectral range. Nevertheless, more recently, the explosion of "generalized plasmonics" has stimulated the search of alternative building block materials [8, 36] that could overcome (or at least compete with) Au and Ag for plasmonic applications in the near UV-to-near IR region, allow plasmonic effects in a wider spectral range (from the VUV to the THz), or present active plasmonic functionalities, i.e. that can be modulated for instance by heating/cooling, optical or magnetic excitation. The key information required for determining the possibilities offered by a given building block material is contained in the real and imaginary part of its dielectric function that must present negative values of ε_1 and values of ε_2 compatible with the desired plasmonic property (excitation of surface plasmon polaritons (SPP), localized surface plasmon resonance (LSPR)-induced absorption or field enhancement, LSPR refractive index sensing). Particularly desired materials are those with low losses, i.e., which present a low or even zero [37] value of ε_2.

The dielectric function of a given building block material depend on the fabrication conditions. This is true even in the case of the broadly studied Ag and Au, whose crystallinity, purity, porosity, or roughness depend on the fabrication process, thus, making the properties of the obtained material depart from those of its perfect crystal counterpart. Evaluation of the dielectric response of Ag, Au, and the many other possible building block materials for plasmonics obtained using given fabrication conditions is the key to the design of novel or optimized plasmonic devices. As plasmonic NSs are often obtained by combining lithography and thin film deposition techniques, great attention has been given to the characterization by SE of building block materials for plasmonics under the form of thin films. Also, due to its capability for *in situ* measurements, SE has been frequently used for the characterization of temperature-sensitive materials and particularly for the study of the phase transition-induced changes in their dielectric function. Such changes are indeed desired for the development of temperature-sensitive, active plasmonic devices.

4.1 Optimizing the properties of building block materials for plasmonic applications

The potential of a broad range of metals, alloys, intermetallics, and some liquid metals for plasmonic applications has been reviewed recently by Blaber et al. [38], based on dielectric functions taken from the literature and not necessarily measured by SE. Among them, the dielectric properties of Au and Ag have been studied early by optical means – mainly by traditional reflectance or transmittance measurements and scarcely by SE (see refs. [39] and [40] for

recent reviews of papers devoted to these two metals) – and the trends of their dielectric functions are now well known. Interband transitions are excited in the UV for Ag and up to visible wavelengths for Au. For wavelengths their respective interband threshold, both behave as Drude-like metals with a negative ε_1 and a reasonably low ε_2, so that moderately lossy plasmonic properties can be expected in the whole visible range for Ag and in part of the visible range for Au. It is a fact that the fabrication conditions of these two metals affect their crystallinity, porosity, and purity thus making their dielectric properties departing from the picture of a pure perfect crystal and varying sufficiently strongly so that the properties of a device built from them could be drastically affected. For example, grain boundaries in polycrystalline Au NPs have been shown to induce an increase in ε_2 for the metal and thus increased nonradiative losses in Au nanoantennas [41]. The broad dispersion of data found in the literature for Au grown by several routes has been underlined in a recent article [40]. In this work [40], SE measurements have been performed using modern setups in a wide spectral range (wavelengths from 300 nm to 25 μm) on Au single crystals and evaporated films with a rough and a flat surface, and the pseudo-dielectric function of the materials (i.e., assuming that they behave as a bulk including the roughness layer) have been extracted. It has been concluded that the broad dispersion of previously reported data may arise mainly from errors in the measurements. Besides, the effect of template stripping on the SE-determined pseudo-dielectric function of Ag thin films deposited by thermal evaporation has been demonstrated [42], showing a decrease in the pseudo-ε_2 in the visible range when surface roughness decreases as a consequence of stripping. To be reported is also a very recent article, devoted to Al, which is particularly interesting for plasmonic applications in the UV due to its low ε_2 values in this spectral range. In this work [43], SE measurements have been performed in a modified Otto configuration in the near UV-to-near IR range on Al single crystals and on thin films grown by several different techniques (evaporation, sputtering, MBE...). The extracted dielectric function of the Al material has been shown to depend strongly on the fabrication route used.

An even more drastic effect of the fabrication conditions may occur in the case of complex building block materials for plasmonics, such as metal-based nitrides, whose dielectric function depends strongly on their composition. Such compounds have been studied earlier by SE under the form of thin films [44–50], and recently, those displaying a Drude-like behavior have been shown to be of interest for plasmonic applications in the visible and near IR [51, 52]. Note that in these recent works [51, 52], the thin films were elaborated by pulsed laser deposition using conditions chosen to minimize optical losses detrimental to plasmonic applications (dense, homogeneous films with smooth surface). An extensive review about the plasmonic potential of metal-based nitrides and a wider range of materials has been reported by Naik et al. [8].

4.2 Transparent conducting oxides for active plasmonics

Early interest has been devoted to transparent conducting oxides for thin-film transparent electrode applications [53–59]. Relevant electrical conductivity can be achieved in oxides (for instance ZnO, In_2O_3, SnO_2) upon impurity doping. The doping-induced dielectric properties have been investigated by SE in the near UV-to-near IR range in textured, nano/microcrystalline oxide thin films as a function of the dopant concentration and nano/microstructure [56–59]. It has been shown that the materials' optical band gap absorption threshold red-shifts upon doping, whereas the Drude contribution to the dielectric function becomes more and more sizeable in the near IR as a consequence of the free-charge carrier concentration increase. "Optical" free-charge carrier concentration and mobility have been extracted from the Drude contribution, using carrier effective mass values derived from electrical Hall measurements [57–59]. In contrast with electrical Hall measurements, SE on the nano/microcrystalline oxides gives access to the in-grain carrier mobility. More recently, and as a consequence of their marked dopant concentration-dependent Drude behavior, transparent conducting oxides have been identified by means of SE measurements as promising tunable compounds for plasmonics [8, 60]. Near-IR plasmonic properties can be achieved with a sufficient doping-induced free-charge carrier concentration, the decrease in which allows driving the range of the plasmonic response further in the IR. For instance, a mid-IR plasmonic behavior has been reported for intrinsic ZnO films using an ellipsometer in the Kretschmann configuration [61]. In fact, the possibility of tuning the plasmonic response of transparent conducting oxides through their free-charge carrier concentration have made them powerful building blocks for the realization of active electrochromic plasmonic nanostructured materials [62].

4.3 Plasmonic effects beyond Drude electrons: the case of bismuth

Generally, following the well-known picture established for Au and Ag and many other plasmonic building block

materials, plasmonic effects are caused by the excitation of Drude-like electrons, with increased losses (in addition to the intrinsic loss of the Drude function) in the spectral range where interband transitions occur. Nevertheless, the observation of plasmonic-like effects (i.e., that mimic some effects encountered with more or less lossy plasmonic metals) has been shown recently to be possible in a wider range of cases, for instance by hole injection in semiconductor NPs [63, 64], or even in the absence of free carriers. Indeed, as explained by Zhu et al. [65] and highlighted by Naik et al. [8], negative ε_1 values can be obtained at the spectral vicinity of a peaked loss band in the ε_2 spectrum. Such a behavior may be at the origin of the (lossy) LSPR-like behavior of Bi NPs that has been observed experimentally in the near UV-visible range and reproduced by simulations [66]. Bi is a low-cost semi-metal with peculiar properties, such as an extremely low bulk free carrier density with a mean free path in the micrometer range at low temperature, a semi-metal to semiconductor transition in nanostructures of several tens of nanometers, a high density of surface state-induced free charge carriers in ultrathin films, and a good but unexploited potential for thermo-optical applications due to its relatively low melting point (~270°C). Despite these properties, the optical response of Bi NPs remains largely unknown and has to be explored. In view of the extremely low free-charge carrier density, it would be very unlikely that the presence of the LSPR-like bands observed in the near UV-visible spectra of Bi NPs [66] had a Drude origin. Instead, it is worth noting that the dielectric function of pulsed laser deposition-grown Bi thin films obtained from UV-visible-near IR SE measurements show (in agreement with earlier studies) the presence of an intense interband loss peaking in the near-IR region of the ε_2 spectrum [66]. This dielectric function was extracted by direct inversion (pseudo-dielectric function) of the ellipsometric spectra of a smooth film whose thickness was larger than the optical skin depth. Deconstruction of the obtained complex dielectric function on the basis of phenomenological Kramers-Krönig-consistent Tauc-Lorentz oscillators, as shown in Figure 3, supports the fact that the negative ε_1 values observed in the visible may be linked with the strong near-IR loss band in virtue of the causality principle. Let us remark that the trends of this Bi dielectric function is comparable to that of Ag or Au in the visible range, however, with higher ε_2 values. In the near IR, in contrast with noble metals, ε_1 takes positive values for Bi thus confirming its non-Drude behavior in this spectral region. Similar features are observed in the dielectric responses of semiconductors such as Si, Ge, GaN, or SiC [67–70]. Besides, the free carrier-induced plasmonic behavior of Bi is expected in the far IR to THz region [19], due to its extremely low carrier density.

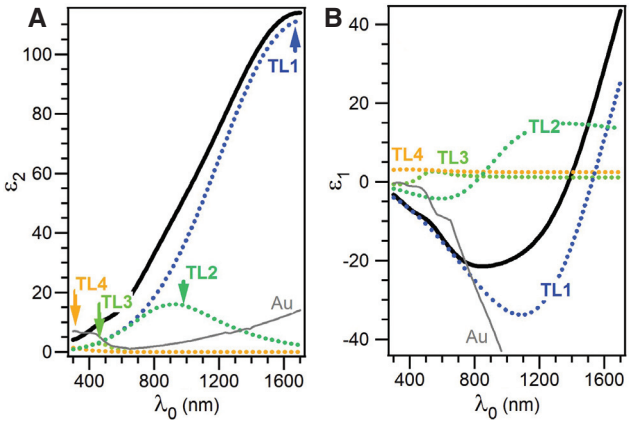

Figure 3 Deconstructing the dielectric function of solid Bi in the near UV-to-near IR range. Spectra of the imaginary part ε_2 (A) and real part ε_1 (B) of the dielectric function of solid Bi (thin film grown by pulsed laser deposition, data taken from [66] – black lines) and real and imaginary part of its Kramers-Krönig-consistent Tauc-Lorentz components (TL1, TL2, TL3, TL4). The spectra are dominated by TL1 that accounts for the strong loss band peaking around 1700 nm (ε_2 spectrum) and the negative ε_1 values in the near UV-to-near IR. The dielectric function of Au taken from the Palik database is also shown (gray lines).

4.4 Temperature-dependence, phase transitions for active plasmonics

SE has been performed *in situ* for evaluating the dielectric function of metals or metallic compounds as a function of temperature, below and above their melting point [39, 49, 71–84]. It has been used early to measure, in the near UV-to-near IR spectral range, the dielectric function of the liquid phase of metals with a low melting point, such as Na, Sn, Hg [71], and later that of Ga in its solid [72] and liquid [72, 73] state, that of Bi in its solid [66] and liquid [73, 74] state. Ref. [73] reviews earlier works about the optical response of Bi and Ga and reports measurements on the liquid phase as a function of temperature. Ref. [74] reviews earlier works and provides new data about the optical properties of solid and liquid Pb. From these works, it comes that the material's dielectric function changes at the phase transition, with a marked decrease of the interband contributions [72, 74], as exemplified in Figure 4A for Bi. Thanks to the optical contrast between the solid and liquid phase, 1D Ga gratings with switchable (SPP) plasmonic properties in the visible have been obtained [72]. Optically monitored temperature sensing based on reversible melting-solidification of Bi NPs

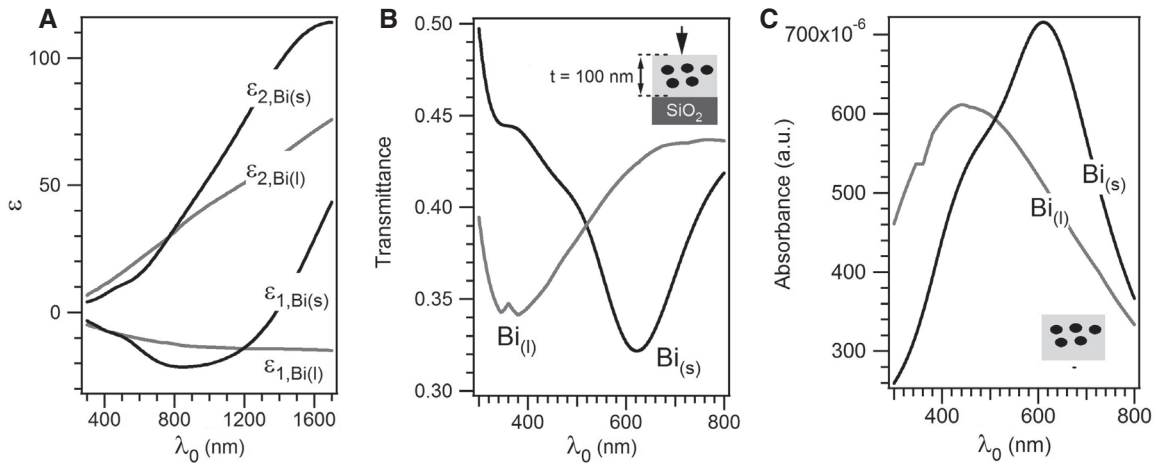

Figure 4 Optical contrast based on the solid-liquid transition of Bi NPs. (A) Real and imaginary part of solid Bi (taken from [66]) and of liquid Bi (interpolated from data taken from [74]). (B) Simulated transmittance spectra (at normal incidence) of a 100-nm-thick film consisting of solid Bi NPs (black line) and liquid Bi NPs (gray line) having the dielectric functions shown in (A), and being embedded in a transparent dielectric matrix described by a Cauchy law with parameters An=2.5, Bn=0.01. The effective in-plane properties of the film were calculated using the extension of the Maxwell-Garnett model to spheroidal NPs with their revolution axis perpendicular to the film surface. The transmittance was derived from the obtained effective dielectric function in the Abelés matrix formalism. The NPs were assumed to be spheroidal, with an oblate shape (H/D ~0.46, i.e., an in-plane depolarization factor L_{xy}=0.2), and a low volume fraction f=5%. The substrate is transparent SiO_2. This figure exemplifies the consequence of the phase transition on the optical response of the sample. (C) Calculated absorbance $\alpha=4\pi k_{eff}/\lambda_0$, k_{eff} being the effective in-plane extinction coefficient of the film, showing that the phase transition affects mainly the optical absorption.

embedded in an inert matrix has been reported in the visible [75]. Further improvement of the optical contrast in such Bi NP-based films can be achieved upon tuning their thickness, composition, and nanostructure. For instance, Figure 4B shows a strong optical contrast in the visible range (relative change up to 37% at 620 nm) between the simulated transmittance spectra of a nanocomposite film consisting of liquid NPs embedded in a high-index transparent matrix and that of the same film containing solid NPs. The observed contrast is due to a strong difference (more than 200 nm) between the spectral positions of the extinction bands observed in the case of solid and liquid Bi NPs. The in-plane effective dielectric properties of the film have been calculated using the extended Maxwell-Garnett effective medium model, assuming that the NPs are oblate spheroids with their revolution axis perpendicular to the film surface, with a height-to-diameter ratio H/D of ~0.46 and present a low volume fraction f=5%. The dielectric functions used for the solid and liquid NPs were those of the corresponding bulk materials shown in Figure 4A. The observed contrast is mainly due to the different absorption spectra of the liquid and solid NPs (the film reflectance is weakly dependent on the dielectric function of the NPs), as proved by the absorbance spectra displayed in Figure 4C. Also, as the volume fraction is low, the optical contrast can be explained mainly as a single-particle effect, i.e., it is driven in this case by the shape of the NPs, their dielectric function in the solid and liquid state, and that of the matrix. At this point, it is worth noting that relevant differences exist between the dielectric functions of solid and liquid Bi in the visible range, as shown in Figure 4A. Indeed, in the 300 nm to 750 nm range, the ε_2 values of liquid Bi are some tens of % higher than those of solid Bi. Also, above 500 nm, ε_1 of the solid Bi decreases fast as a function of λ_0, its absolute value being twice that of liquid Bi at 800 nm. The spectra of both ε_1 and ε_2 affect the resonance condition of the NPs: therefore, liquid and solid Bi NPs are expected to present resonances at different wavelengths. However, in contrast with Ag or Au that present low and almost wavelength-independent ε_2 values in the visible range, no simple condition can be derived for the resonance wavelength of the Bi NPs. Therefore, the optical contrast between the nanocomposite with liquid Bi and that with solid Bi is a nontrivial function of the NP shape, of their dielectric functions and of that of the matrix. Discussing this relation shall be the subject of further works, beyond the scope of this review. SE-based works have also been devoted to the wetting transitions at the surface of Ga-Bi alloys [73, 76], to surface freezing in Ga-based alloys [77], and to wetting and prewetting transitions at the metal-rich K-KCl melt-sapphire interface [78, 79]. SE measurements at higher temperatures (up to 1350°C) have also been performed from the visible to the far IR on molten metals [80–84].

Much attention has also been devoted to the SE characterization of the dielectric function of vanadium oxides, VO_2 [85–88] and V_2O_3 [88, 89], from the near UV to the far IR and at different temperatures, in order get insights into the parameters driving their insulator-to-metal transition occurring at moderate temperature. In the case of VO_2 especially, this transition induces a marked change in the dielectric function in the IR (ε_1 turns from positive to negative) that has attracted interest for plasmonic applications. Indeed, due to the change in sign for ε_1 in the IR, suitably designed VO_2 NSs have been observed to turn (with a very fast time response) from nonplasmonic to plasmonic in this spectral range [90, 91], VO_2 being thus an interesting building block material for active plasmonics. This property has been used to propose improved designs for VO_2-based smart windows, standing on the optical absorption by localized surface plasmon resonances in VO_2 NPs above the transition temperature [92]. VO_2 can also be used as an active matrix for switching the response of plasmonic NSs of other nature [93].

SE has also been of great help for the determination of the dielectric properties of the different phases (amorphous, crystalline, liquid) of many phase-change compounds (under the form of bulk or thin films) in the visible-near IR range for data storage applications [94–98]. For many of them, one phase displays negative values for ε_1 and the other phase, positive values. As it is the case for Bi (as discussed above), the negative ε_1 values have a non-Drude origin [94]; also, NSs presenting such ε_1 values, together with those reported for ε_2, may induce damped LSPR-like resonances in the visible range.

5 Ultrathin films

When the thickness of a film is decreased to a few nm (the ultrathin film limit), its dielectric function may be thickness dependent. SE has been shown early to be sensitive to the presence of ultrathin films on a substrate [99, 100]. As shown in Figure 2C, the Δ spectrum is strongly affected when an ultrathin overlayer is grown. The thickness dependence of the dielectric properties of ultrathin films may have several different origins such as confinement-induced effects in smooth films [5, 101] or a discontinuous nanostructure of the film. The latter effect is frequently encountered in the first stages of Volmer Weber-like growth where isolated NPs first grow on the substrate until percolation is reached and a continuous film finally forms. SE allows to monitor *in situ* the different stages of discontinuous growth [6, 102–105], and permits to evidence the percolation threshold [6, 104, 105]. Near UV-to-near IR SE has been used to characterize *in situ* the temperature-dependent response of Ag NPs grown on a substrate [106], and recent *in situ* near UV-to-near IR SE studies on supported Ga or Ga-Mg NPs are to be highlighted [107–111] due to the potential of these materials for active plasmonics. It is worth noting here that SE measures the effective properties of a macroscopic area of the discontinuous film. Conversion of this effective data into information about the nanostructure of the film, or the dielectric properties of individual NPs requires modeling, for instance, in the framework of effective medium theories. Using simple effective medium models such as that of Bruggeman has allowed to get precise nanostructural information, for instance, in the context of nanoscale surface roughness evaluation [112]: in this case, surface roughness is usually considered as an ultrathin granular film on top of a homogeneous material. Nevertheless, in many cases, more complex models or even full numerical approaches have to be used [6, 26]. As it will be detailed in the next section, the use of appropriate modeling is mandatory for an accurate quantification confinement-induced effects in NSs from macroscopic SE measurements.

6 Small-size effects in nanostructures

The dielectric properties (described by their dielectric function ε_{NS}, or tensor $[\varepsilon_{NS}]$) of NSs often differ from those of the corresponding bulk material, due to classical or quantum effects. Early and recent works have aimed at the observation of the so-called small-size effects from macroscopic measurements on statistical assemblies of NSs, deposited on a substrate or embedded in a protective matrix. The measured quantity is typically the effective response of a nanocomposite medium (air:NSs/substrate, NSs:matrix) given by ε_{eff} (or $[\varepsilon_{eff}]$) [113], which is affected by ε_{NS} (or $[\varepsilon_{NS}]$), by the shape, organization of the NSs, and the nature of the substrate or surrounding matrix [113, 114]. Therefore, as explained below, the accurate determination of ε_{NS} from ε_{eff} requires appropriate modeling, together with the fabrication of model materials with a well-characterized nanostructure.

6.1 Confinement in semiconductor nanoparticles: the case of silicon

Besides the strongly desired indirect-to-direct band-gap transition for c-Si as a consequence of quantum

confinement in NPs a few nm in size, theoretical works have predicted a decrease in the static dielectric function of c-Si, in relation with the expected size-induced widening of the band gap and a lower polarizability due to surface effects. Experimental efforts have thus been made in order to determine, by optical means, the dielectric function ε_{NS} of Si NPs, especially in the spectral range of their band gap absorption that is of importance for photovoltaic or photoluminescence sensitization applications. Owing to their extremely small size, the dielectric response of such Si NPs can, however, hardly be studied on a single particle. Instead, optical measurements using macroscopic probes have been performed on nanocomposite materials consisting of statistical amounts of Si NPs deposited on a substrate or embedded in transparent matrix. In order to study the dependence of ε_{NS} on the NP size, nanocomposite materials containing c-Si or a-Si NPs with a controlled average size were fabricated and their effective dielectric function ε_{eff} measured by near UV-to-near IR SE. Then, ε_{NS} was extracted using effective medium models [115–128]. The volume fraction f and average size of the NPs reported in these works span over a wide range (from 1% to 40% with strongly different organizations of the NPs within the matrix, and from 1.5 nm to 10 nm, respectively), as well as the values of ε_{NS}. Keita et al. [129] gathered some of the data given in these works, and observed that, although the features related with optical transitions (for instance critical points) can be damped or shifted with respect to the bulk, no general and explicit size dependence for ε_{NS} could be deduced. As possible explanation to this absence of correlation, they underlined a weak point of the effective medium models used to extract ε_{NS}, i.e., they neglect the NP size distribution, which is in fact significant in most of the previously published works. They therefore proposed an effective medium model that takes size distributions into account [129, 130] and showed the drastic effects of even a moderate polydispersity on the effective optical band-gap absorption. Inhomogeneous broadening leads to a loss of information, thus, meaning that almost monodisperse assemblies of particles must be grown [131] in order to study the correlation between ε_{NS} and the NPs size. Also, effective medium modeling in the reported works [115–128] was done mainly using the basic monodisperse Maxwell-Garnett or Bruggeman theories (which are extremely crude models, rigorously adequate only in some cases involving 3D assemblies of NPs) irrespectively of the organization and volume fraction of the NPs. Owing to the very different features of these two theories and their simplicity, the examination of their suitability to the accurate description of the nanocomposite materials under study might be an important issue. Figures 5 displays effective dielectric functions calculated using both theories for spherical Si NPs embedded in a transparent matrix with a volume fraction f=20% and indeed shows that a relevantly different effective response is obtained using the two models. Such

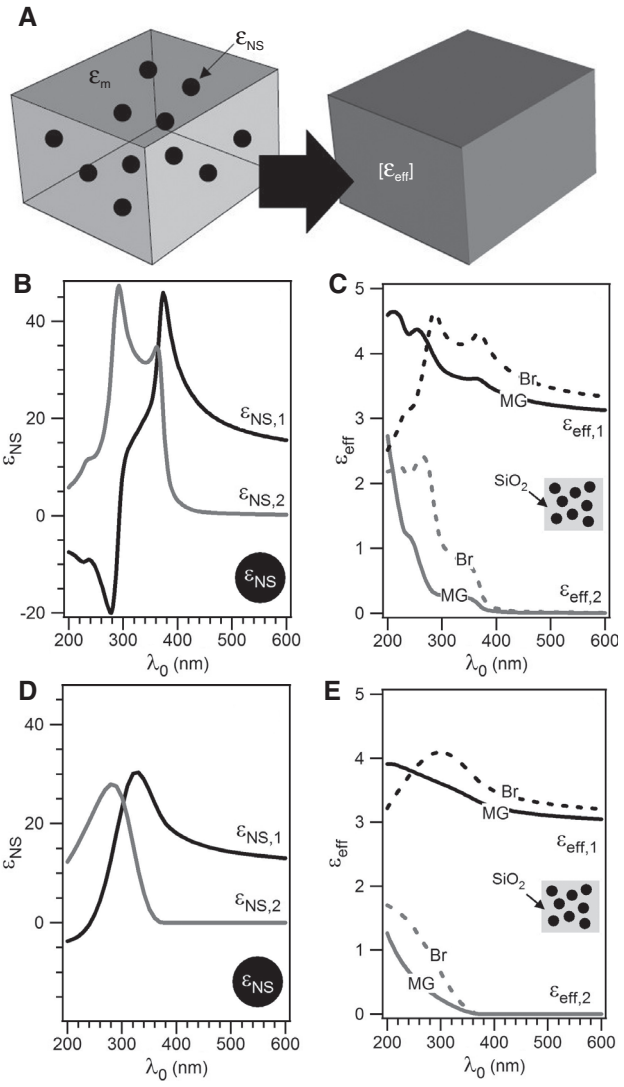

Figure 5 The effective dielectric function of assemblies of embedded Si NPs – model dependence. (A) Schematic representation of a nanocomposite medium and its effective equivalent. (B) Real and imaginary part of the dielectric function of Si (data taken from the Palik database), taken for the dielectric function ε_{NS} of the NPs in (C), and (D) real and imaginary part of a dielectric function typical of some of those found in the literature for confined Si (see ref. 129), taken for the dielectric function ε_{NS} of the NPs in (E). (C) and (E) Real and imaginary part of the effective dielectric function ε_{eff}, of a composite medium consisting of NPs with the dielectric function ε_{NS} shown in (B) and (D), respectively, embedded in a SiO_2 transparent matrix. Calculations have been performed using the Maxwell-Garnett (MG) and Bruggeman (Br) models, assuming spherical NPs and a volume fraction f=20%. It can be seen that both models yield very different results both for the real and imaginary part of ε_{eff}.

a difference is observed whether the intrinsic response of the NPs is described using the bulk dielectric function of Si (Figure 5B and C) or a damped dielectric function qualitatively comparable to those found in the literature for Si NPs a few nm in size (Figure 5D and E). The Maxwell-Garnett effective medium model is based on calculations of the local electrostatic field at a given NP in the Lorentz sphere approximation. This NP is located at the center of the Lorentz sphere, which is made of the matrix material (dielectric function ε_m) and is surrounded by the effective material (dielectric function ε_{eff}). Therefore, this model is a good approximation in cases where the interaction between neighbor NPs does not need to be described using exact calculations of their scattered fields, i.e., for instance when these fields are very weak. In contrast, the Bruggeman effective medium model assumes that two types of inclusions, one with the dielectric function of the Si NPs (ε_{NS}) and the others with the dielectric function of the matrix (ε_m), are embedded in the effective medium (ε_{eff}). This model is therefore more appropriate when the NPs and the matrix can be treated in a symmetric manner. From these qualitative considerations, it seems that the response of dilute assemblies of Si NPs a few nm in size, whose near field is very weak, might be better described using the Maxwell-Garnett model. Further quantitative work is required in order to discuss this point and to determine in which conditions (on f, ε_m, ε_{NS}) each of these models can be used legitimately as far as Si NPs are concerned and when other models should be employed. In addition, the real NP shape and organization (described more accurately than by a volume fraction) might have to be taken into account in some cases. Also, the local environment of the NPs may play a role on their size-dependent response. Therefore, it may be that some work remains to be done in order to determine in an accurate manner the size dependence of the dielectric response of Si NPs and, more generally, that of semiconductor NSs.

6.2 Small-size effects in metal nanoparticles

Small-size effects in metal NPs have long been studied theoretically and experimentally [131], especially for noble metals. Although the main trends governing the size dependence of the optical response of Au and Ag have been much debated, obtaining more accurate experimental data from studies on model materials [132, 133] is still desirable. In principle, size effects in metal NPs are observed through the evolution of the position and width of their LSPR(s). Such evolution may be linked with effects involving directly the conduction electrons (such as surface scattering, chemical interface damping [131, 133]) or through their interaction with other excitations affected by small-size effects. Indeed, small-size effects on the interband transitions have also been evidenced [134–136]. From the features of the LSPR(s), the dielectric function ε_{NS} or dielectric tensor [ε_{NS}] of the NPs can be extracted provided all the other parameters (NPs shape, size, environment) are known. Nevertheless, it is worth noting that this procedure, if accurate in the spectral region of the

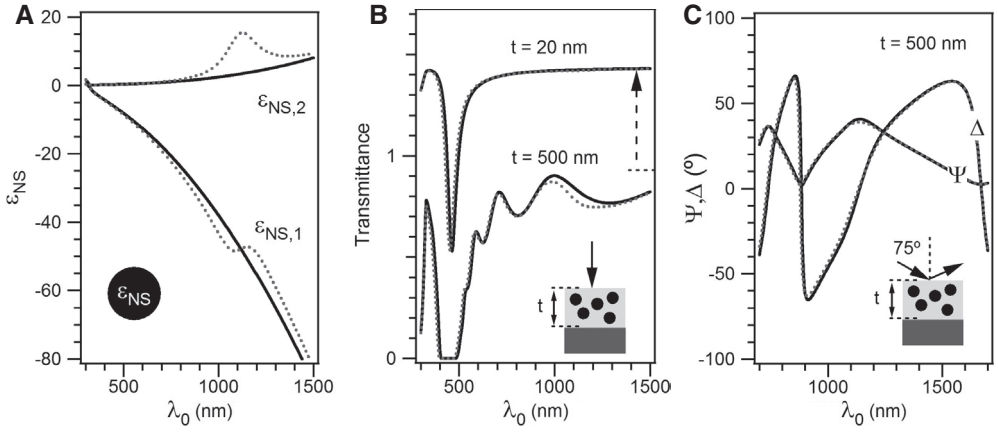

Figure 6 Determining the dielectric function of plasmonic NPs – intrinsic limitation of optical measurements. (A) Real and imaginary part of the dielectric function ε_{NS} of fictitious NPs, with a Drude-like behavior (dark full lines) or with a Drude-like component plus a Lorentz peak, centered at 1120 nm (gray dotted lines). (B) Transmittance spectra of effective media (deposited on a SiO_2 substrate), calculated in the Maxwell-Garnett approximation assuming spherical NPs with the dielectric functions ε_{NS} defined in (A) embedded in a transparent matrix (ε_m=2.72) with a 10% volume fraction. Two thicknesses t (20 nm and 500 nm) have been chosen for the effective medium. Plasmon resonance is observed around 450 nm. (C) Calculated ellipsometry spectra (75° incidence) for the effective media defined in (B) (deposited on Si). The Lorentz peak contribution to ε_{NS} affects in an extremely weak way T, Ψ and Δ in the NIR range, so that a clear graphical evidence of its influence in this range can be noticed only in the T spectrum of the 500-nm-thick film.

LSPR(s), may be less appropriate away from this region, as shown in Figure 6. Determining ε_{NS} in a broader spectral range may therefore require to make assumptions on its spectral evolution or to tune the material structure in order to make its influence on the effective response stronger. Another possible way to be followed consists in tuning the NP environment (without altering their interface, size, shape, and avoiding electrical contact between them) in order to make the resonance(s) shift.

7 Metamaterials

During the last decade, an increasing interest has been devoted to metamaterials engineering, aiming at exciting properties, such as light trapping [137], tunable birefringence or dichroism [138], effective optical magnetism or chirality, and negative refraction from the IR range to the visible [139]. SE has proved to be an interesting tool for the investigation of the electromagnetic properties of these materials.

7.1 2D assemblies of nanoparticles

Standard SE in the near UV-to-near IR range has been used to determine the effective dielectric response of 2D assemblies of Ag NPs embedded in a dielectric matrix (as schematized in Figure 7A) with polydisperse ellipsoidal shapes [137, 140] and an isotropic in-plane organization,

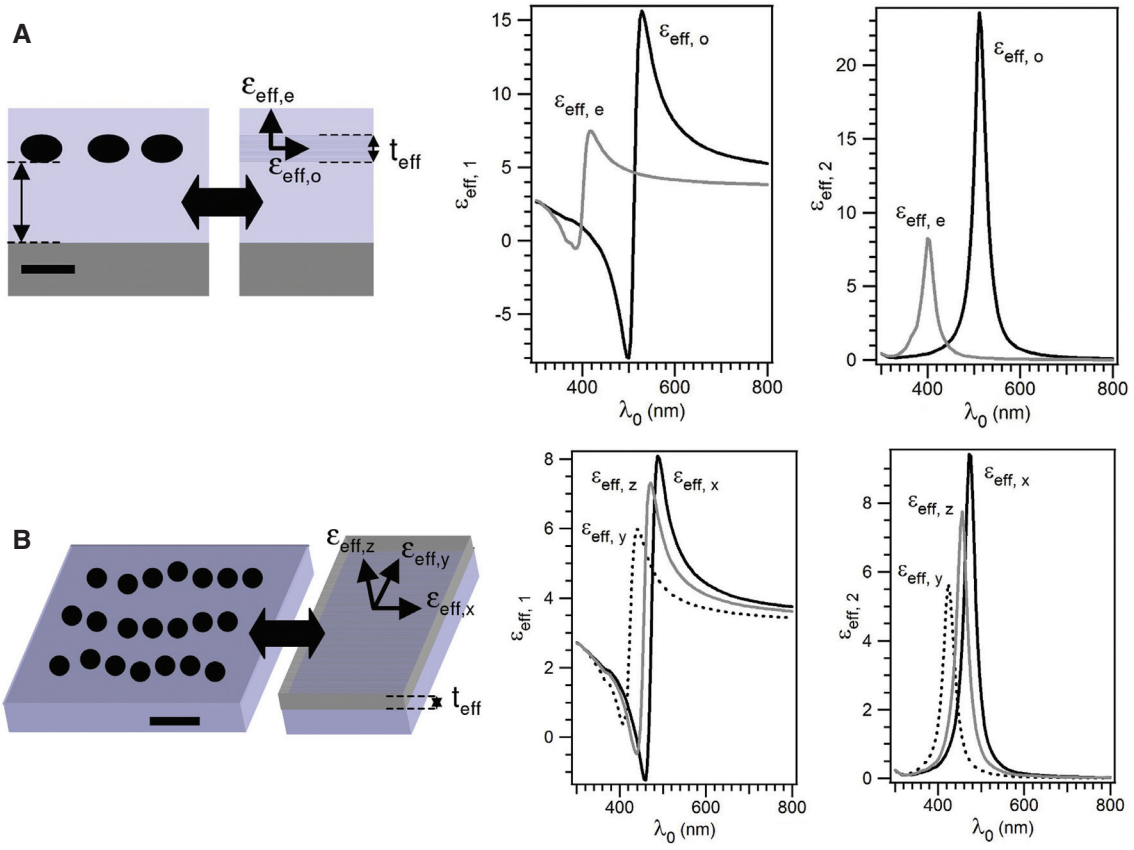

Figure 7 Examples of plasmonic metamaterials described in the Abélès matrix formalism using the effective medium approximation. Schematic representation of (A) a 2D assembly of NPs embedded in a dielectric matrix (seen in cross-section); (B) Planar assembly of 1D arrays of aligned NPs on a substrate. Typical order-of-magnitude scale bars are also shown: 10 nm for (A), 20 nm for (B). Their effective counterparts are also depicted, together with the parameters (dielectric functions, effective thickness t_{eff}) that can be extracted from measurements. Effective medium simulations of the real and imaginary part of the corresponding dielectric functions are also shown in each case. In (A), the simulations have been done using the Yamaguchi theory, assuming oblate spheroidal Ag NPs with a vertical revolution axis (with the bulk silver dielectric function taken from the Palik database) embedded in a-Al_2O_3 (transparent matrix with an index of 1.65), aspect ratio H/D=0.5, diameter D=10 nm, interparticle distance L=20 nm. In (B), the simulations have been done using a biaxial extension of the Yamaguchi theory, for spherical Ag NPs (D=10 nm) distributed in a plane and embedded in a-Al_2O_3, with an interparticle distance L_x=15 nm along the aligned NPs and L_y=50 nm between the 1D arrays of NPs.

which can be included in vertical photonic structures for highly efficient light harvesting. Standard near UV-to-near IR SE measurements on 2D assemblies of supported Au nanodisks fabricated by nanolithography have also been reported [141]. As a consequence of the 2D organization and in-plane flattened/elongated shape of the NPs, these systems present a uniaxial dielectric response, with a vertical optical axis. Effective medium modeling based on extensions of the Yamaguchi effective medium theory has shown reasonable agreement with the experimental data [140, 141]. An example of uniaxial anisotropy predicted by the Yamaguchi effective medium theory is shown in Figure 7A, in the case of a 2D in-plane isotropic distribution of oblate Ag NPs with a vertical revolution axis, embedded within a transparent matrix. LSPR modes peaking at distinct wavelengths are excited in the plane (ordinary effective dielectric function $\varepsilon_{eff,o}$) and perpendicularly to it (extraordinary effective dielectric function $\varepsilon_{eff,e}$) due, in this case, mainly to the shape anisotropy and specific orientation of the NPs. Uniaxial effective dielectric anisotropy has also been observed in the case of supported 2D assemblies of Au nanodisk/SiO_2 nanodisk/Au nanodisk, together with Fano features related to the interference between waves scattered by the weakly interacting Au nanodisks [142]. In the case of a stronger coupling between disks in the sandwich structures, optical magnetism has been reported [143]. Besides, in-plane and out-of-plane effective anisotropies have been tracked by near UV-to-near IR standard SE measured at several azimuths on 1D arrays of aligned Ag NPs deposited on stepped substrates [144, 145] (schematized in Figure 7B). By means of near UV-to-near IR Mueller matrix-generalized SE measurements, a biaxial effective dielectric tensor has been extracted for 1D arrays of aligned Ag NPs deposited on rippled surfaces [146], showing in-plane effective plasmonic birefringence and dichroism. Figure 7B shows an example of biaxial anisotropy in a planar assembly of 1D arrays of Ag NPs embedded in a transparent matrix, based on simulations obtained using the biaxial extension of the Yamaguchi effective medium theory. LSPR modes peaking at distinct wavelengths are excited along the x, y (in-plane) and z (vertical) directions, this time as a consequence of the NP organization only (the NPs are spherical).

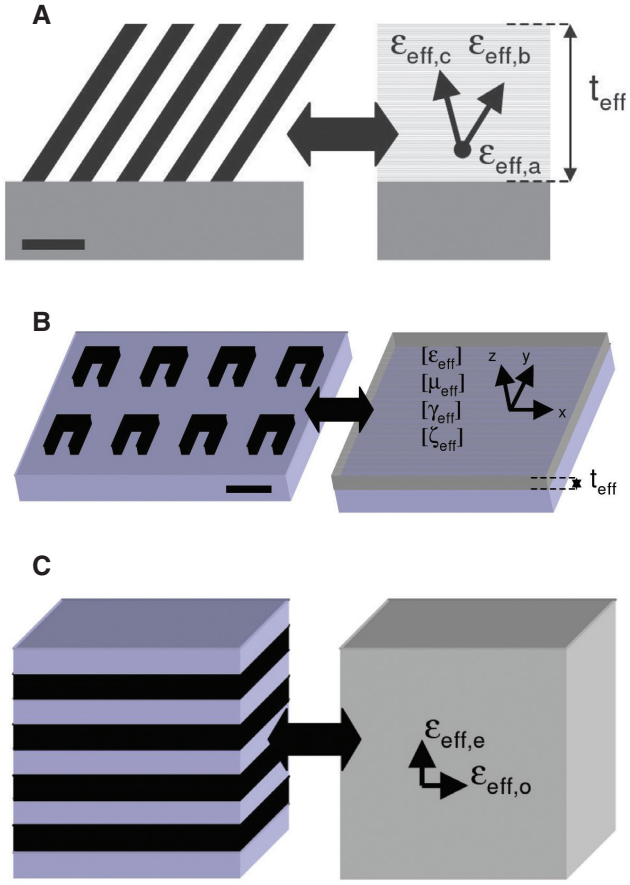

Figure 8 More metamaterials – biaxial anisotropy, optical magnetism, and hyperbolic material. Schematic representation of (A) a thin film consisting of slanted nanocolumns; (B) a 2D assembly of supported U-shaped resonators; (C) a multilayered hyperbolic metamaterial. Their effective counterparts are also depicted, together with the parameters that can be determined from measurements. In (A), these parameters are the orientation of the principal axes of the dielectric tensor, its diagonal components, the film effective thickness. In (B), the effective thickness and the four constitutive tensors (dielectric permittivity [ε_{eff}], magnetic permeability [μ_{eff}], chirality [γ_{eff}], and [ζ_{eff}]). In (C), the effective ordinary $\varepsilon_{eff,o}$ and extraordinary $\varepsilon_{eff,e}$ dielectric functions. Typical order-of-magnitude scale bars are also shown: 50 nm for (A), 200 nm for (B). In (B), the principal axes in which the constitutive tensors are expressed are shown. In (C), the multilayer period must be small compared to the wavelength of incoming waves so that effective medium approximation is valid.

7.2 Slanted nanocolumnar thin films, chevron, and chiral structured thin films

Thin films of slanted nanocolumns (see schematic representation in Figure 8A) have attracted much interest. A comprehensive review about such systems is given in ref. [7]. The normal-incidence optical properties of Ag slanted nanocolumnar films display a strong in-plane dichroism and have been claimed to be equivalent to those of an effective material with a negative real refractive index [147]. Generalized SE has been extensively performed in the near UV-to-near IR (mainly in the framework of Mueller matrix SE) on thin films of slanted nanocolumns. It gives access nondestructively to the film thickness, to the principal coordinate system of the biaxial anisotropic effective material (and thus to the

orientation of the nanocolumns), and to the components of the material's (diagonal) effective dielectric tensor in this coordinate system. An orthorhombic symmetry has been evidenced in the case of a-Si:SiO_2 nanocolumns [148] and a monoclinic symmetry in the case of Cr [149], Ti [150], Co [151] nanocolumns. Issues about the effective medium modeling of such films have been discussed [152]. Mueller matrix-generalized SE in the near UV-to-near IR has also proved to be sensitive to the presence of polymers infiltrated into the pores between silicon [153] or permalloy [154] nanocolumns. Infiltration/swelling of the polymer leads to an increase in the tilt angle of the nanocolumns. Mueller matrix-generalized SE together with microbalance nanogravimetry have shown to be adequate for the determination of adsorption isotherms on slanted nanocolumnar TiO_2 thin films [155]. Mueller matrix-generalized SE measurements of the THz effective dielectric anisotropy on Co-slanted nanocolumnar thin films have also been reported [156]. In addition, near UV-to-near IR Mueller matrix SE measurements have been performed on chevron structured thin films [157] and chiral nanoporous silver thin films [158].

7.3 Fishnet structures, split ring resonators, U-shape resonators, 3D metamaterials, and hyperbolic metamaterials

The angular-dependent optical modes of noble metal-based fishnet metamaterials, designed with the aim of obtaining optical magnetism and negative refraction in the visible or near IR, have been characterized by generalized SE [159]. The possibility of defining effective medium parameters for such complex metamaterials has been discussed [160, 161], and it has been claimed that the optical magnetism in these structures cannot be dissociated from spatial dispersion (that makes necessary to describe the materials' response in terms of wave parameters instead of effective tensors) [161]. Mueller matrix SE has also been performed on square arrays of holes in Au thin films [162]. The IR plasmonic modes of assemblies of split ring resonators have been studied by standard SE at two azimuthal angles [163]. Arrays of U-shape resonators (see Figure 8B) displaying resonances in the near IR have been characterized by Mueller matrix SE at three azimuthal angles [164]. From an analysis based on the Berreman formalism and taking into account four characteristic tensors ($[\varepsilon_{eff}]$, $[\mu_{eff}]$, $[\gamma_{eff}]$, and $[\zeta_{eff}]$) for the anisotropic metamaterial, a relatively weak contribution of spatial dispersion (introduced through the addition of tensors elements) was found compared with those of the magnetic and electric resonance modes [164]. Meanwhile, aiming at the fabrication of bulk, isotropic, nondispersive metamaterials presenting effective optical magnetism in the visible, it has been proposed that assembling colloidal plasmonic NPs could be an efficient way to the obtention of optically magnetic isotropic materials. Standard SE has been used for the characterization of plasmonic metamaterials built from colloidal NPs [165, 166]. Besides and finally, the standard SE determination of the dielectric functions of doped InGaAs and intrinsic AlInAs, on the one hand, and ZnO and Al:ZnO, on the other hand, has allowed designing multilayered hyperbolic metamaterials with anisotropic effective properties (see Figure 8C), showing negative refraction in the mid IR [167] and near IR [168], respectively.

7.4 Extracting nanostructural information from metamaterials using spectroscopic ellipsometry

As underlined in Section 3, a reliable characterization of materials by SE requires to choose the setup and the measurement conditions in correlation with the sample to be analyzed and the parameters to be determined. The measurement accuracy, sensitivity to the different parameters and possible correlation between them are also key aspects to be evaluated. These considerations are also true in the particular case of metamaterials. In addition, a model suitable to a physically correct description of the material must be chosen. When the sample under study can be described in the effective medium approximation (which is not always the case), effective constitutive functions or tensors characteristic of the material can be extracted and give a fingerprint of the material's response. As these functions or tensors reflect the nanostructure of the material, it is tempting to extract nanostructural information from them, beyond the effective thickness value (for instance, the shape, size of NPs, or distance between them). At such aim, an effective medium model must be chosen in correlation with the sample, among those cited before (Maxwell-Garnett, Bruggeman, Yamaguchi, and their extensions) or the many others [6, 26] that are suitable to a wide range of cases. In the case where no adequate effective medium model would exist, could be developed, or would the material under study not fulfill the conditions of effective medium approximation, full numerical approaches can be used, however, at a higher computing cost.

7.5 Metamaterial-based detectors with phase sensitivity

Owing to its capability for retrieving amplitude and phase information for the radiation interacting with a material

(through the ellipsometric angles Ψ and Δ, respectively), SE has proven early to be an excellent candidate for sensing applications [169, 170]. The sensing processes are based on the variation of the effective dielectric properties of the material as a function of an external parameter (concentration of a gas, of a chemical agent, temperature, etc.). Recently, monitoring of the SE phase information has shown strong potential for improving the sensitivity of surface plasmon-based refractive index probing and label-free single-molecule detection [171–174]. An important property sustaining this accuracy improvement is topological optical darkness [174], which can be achieved in plasmonic metamaterials. Provided the material structure is adequate, excitation conditions (wavelength, angle) can be found so that Ψ cancels due to a plasmon excitation, and an abrupt change in Δ is observed around the zero Ψ wavelength. This effect has been initially underlined in arrays of Ag NPs displaying collective plasmon resonance modes [173, 174] and more recently on 3D metamaterials assembled from core-shell Ag-SiO_2 NPs [175]. Achieving such an effect in a wider range of plasmonic metamaterials, either in terms of structure or chemical nature, might provide solutions for improving many other sensing applications.

8 Conclusions and outlook

At the present time, the SE technique allows to get effective information about the electromagnetic response in a broad spectral range (from the VUV to the THz) of materials ranging from the simplest case of isotropic homogeneous semi-infinite media to the more complex anisotropic 2D metamaterials. Based on adequate modeling, this information can be converted into knowledge about the material's nanostructure or electronic properties. It is a nondestructive, noncontact technique that can be implemented *in situ*. Owing to the availability of compact and automatized SE setups, it is a candidate of choice for the control and the optimization of industrial processes in real-time, as well as for in-lab characterization. It is also ideal for advanced sensing applications, as combining the phase information provided by SE with metamaterials engineering is an important issue for the development of highly accurate detectors.

In the present context of development of always more finely tailored materials, the interest in SE may therefore keep on increasing. This trend may be even more reinforced by the development of still better systems and computing tools for data acquisition and treatment. Based on these developments, accurate characterization of structured surfaces based on the combination of Mueller matrix SE [176, 177], with scatterometry [178], scatterometry SE [179], other nondestructive/noncontact characterization techniques [180], and numerical calculations [181] is to be foreseen.

However, despite of the rich and still improving capabilities of characterization tools and the existing data analysis software, the user plays a central role either when choosing the measurement conditions or when realizing the essential fitting-based analysis of the recorded data. Indeed, modeling is a central task for obtaining reliable information about the studied material. Therefore, successful use of SE requires the user's expertise to be commensurate with the complexity of the problem to be solved.

Acknowledgments: I strongly acknowledge Pr. Dr. Rosalia Serna for many fruitful discussions. Financial support from the European Commission (FP7 STREP BisNano Project), the Spanish Ministry for Economy and Competitiveness (TEC2012-38901-C02-01 AMALIE), and from the Spanish INEM is also acknowledged.

Received December 22, 2013; accepted February 9, 2014; previously published online March 22, 2014

References

[1] Azzam RMA. The intertwined history of polarimetry and ellipsometry. *Thin Sol. Films* 2011, 519, 2584–2588.
[2] Azzam RMA, Bashara NM. *Ellipsometry and Polarized Light*, Elsevier North Holland Pub. Co.: Amsterdam, 1977.
[3] Tompkins HG, Irene EA. *Handbook of Ellipsometry*, Springer, 2005.
[4] Fujiwara H. *Spectroscopic Ellipsometry: Principles and Applications*, Wiley: Chichester, UK, 2007.
[5] Losurdo M, Bergmair M, Bruno G, Cattelan D, Cobet C, de Martino A, Fleischer K, Dohcevic-Mitrovic Z, Esser N, Galliet M, Gajic R, Hemzal D, Hingerl K, Humlicek J, Ossikovski R, Popovic Z, Saxl O. Spectroscopic ellipsometry and polarimetry for materials and systems analysis at the nanometer scale: state-of-the-art, potential, and perspectives. *J. Nanopart. Res.* 2009, 11, 1521–1554.
[6] Oates TWH, Wormeester H, Arwin H. Characterization of plasmonic effects in thin films and metamaterials using spectroscopic ellipsometry. *Prog. Surf. Sci.* 2011, 86, 328–376.
[7] Losurdo M, Hingerl K. Ellipsometry at the nanoscale. Springer-Verlag: Berlin Heidelberg, 2013.

[8] Naik GV, Shalaev V, Boltasseva A. Alternative plasmonic materials: beyond gold and silver. *Adv. Mat.* 2013, 25, 3264–3294.
[9] Khurgin J, Boltasseva A. Reflecting upon the losses in plasmonics and metamaterials. *MRS Bull.* 2012, 37, 768–779.
[10] Wagner T, Hilfiker JN, Tiwald TE, Bungay CL, Zollner S. Materials characterization in the vacuum ultraviolet with variable angle spectroscopic ellipsometry. *Phys. Stat. Sol. (A)* 2001, 4, 1553–1562.
[11] Kamineni VM, Hilfiker JN, Freeouf JL, Consiglio S, Clark R, Leusink GJ, Diebold AC. Extension to the far UV spectroscopic ellipsometry studies of high-k dielectric films to 130 nm. *Thin Sol. Films* 2011, 519, 2894–2898.
[12] Saenger MF, Höing T, Robertson BW, Billa RB, Hofmann T, Schubert E, Schubert M. Polaron and phonon properties in proton intercalated amorphous tungsten oxide thin films. *Phys. Rev. B* 2008, 78, 245205.
[13] Dubroka A, Rössle M, Kim KW, Malik VK, Schultz L, Thiel S, Schneider CW, Mannhart J, Herranz G, Copie O, Bibes M, Barthélémy A, Bernhard C. *Phys. Rev. Lett.* 2010, 104, 156807.
[14] Tiwald TE, Woollam JA, Zollner S, Christiansen J, Gregory RB. Carrier concentration and lattice absorption in bulk and epitaxial silicon carbide determined using infrared ellipsometry. *Phys. Rev. B* 1999, 60, 11464.
[15] Hinrichs K, Gensch M, Esser N. Analysis of organic films and interfacial layers by infrared spectroscopic ellipsometry. *Appl. Spectro.* 2005, 59, 272A.
[16] Hofmann T, Herzinger CM, Boosalis A, Tiwald TE, Woollam JA, Schubert M. Variable-wavelength frequency-domain terahertz ellipsometry. *Rev. Sci. Instr.* 2010, 81, 023101.
[17] Neshat M, Armitage NP. Developments in THz range ellipsometry. *J. Infrared Milli Terahz Waves* 2013, 34, 682–708.
[18] Schöche S, Hofmann T, Darakchieva V, Ben Sedrine N, Wang X, Yoshikawa A, Schubert M. Infrared to vacuum-ultraviolet ellipsometry and optical Hall-effect study of free-charge carrier parameters in Mg-doped InN. *J. Appl. Phys.* 2013, 113, 013502.
[19] Tediosi R, Armitage NP, Giannini E, Van der Marel D. Charge carrier interaction with a purely electronic collective mode: plasmarons and the infrared response of elemental bismuth. *Phys. Rev. Lett.* 2007, 99, 016406.
[20] Karageorgiev P, Orendi H, Stiller B, Brehmer L. Scanning near-field ellipsometric microscope-imaging ellipsometry with a lateral resolution in nanometer range. *Appl. Phys. Lett.* 2011, 79, 1730–1732.
[21] Tranchida D, Diaz J, Schön P, Schönherr H, Julius Vancso G. Scanning near-field ellipsometry microscopy: imaging nanomaterials with resolution below the diffraction limit. *Nanoscale* 2011, 3, 233–239.
[22] Schubert M, Rheinländer B, Woollam JA, Johs B, Herzinger CM. Extension of rotating-analyzer ellipsometry to generalized ellipsometry: determination of the dielectric function tensor from uniaxial TiO_2. *J. Opt. Soc. Am.* 1996, 13, 875–883.
[23] Schubert M. Polarization-dependent optical parameters of arbitrarily anisotropic homogeneous layered systems. *Phys. Rev. B* 1996, 53, 4265.
[24] Hofmann T, Herzinger CM, Krahmer C, Streubel K, Schubert M. The optical Hall effect. *Phys. Stat. Sol. (A)* 2008, 4, 1179–1183.
[25] Hofmann T, Herzinger CM, Tedesco JL, Gaskill DK, Woollam JA, Schubert M. Terahertz ellipsometry and terahertz optical-Hall effect. *Thin Sol. Films* 2011, 519, 2593–2600.
[26] Toudert J. *Modeling and optical characterization of the localized surface plasmon resonances of tailored metal nanoparticles, in UV-Vis and photoluminescence spectroscopy for nanomaterials characterization*, Kumar C, Ed., Springer-Verlag: Berlin Heidelberg, 2013.
[27] Paulson PD, Hegedus SS. Accurate determination of optical constants of textured SnO_2 using low incidence angle spectroscopic ellipsometry. *J. Appl. Phys.* 2004, 96, 5469–5477.
[28] Necas D, Franta D, Bursikova V, Ohlidal I. Ellipsometric characterisation of thin films non-uniform in thickness. *Thin Sol. Films* 2011, 519, 2715–2717.
[29] Franta D, Necas D, Ohlidahl I. Anisotropy-enhanced depolarization on transparent film/substrate system. *Thin Sol. Films* 2011, 519, 2637–2640.
[30] Soukoulis CM, Wegener M. Past achievements and future challenges in 3D photonic metamaterials. *Nat. Photon.* 2011, 5, 523–530.
[31] Tiwald T. *Metamaterials and the Meta-6 Layer*. J.A. Woollam Co. Inc. Newsletter: Lincoln, Nebraska, USA, 2011, 12.
[32] Rogers PD, Kang TD, Zhou T, Kotelyanskii M, Sirenko AA. Mueller matrices for anisotropic metamaterials generated using 4*4 formalism. *Thin Sol. Films* 2011, 519, 2668–2673.
[33] Chen C, Horn MW, Pursel S, Ross C, Collins RW. The ultimate in real-time ellipsometry: multichannel Mueller matrix ellipsometry. *Appl. Surf. Sci.* 2006, 253, 38–46.
[34] Tiwald TE, VanDerslice J. Method for enhancing sensitivity to out-of-plane properties of uniaxially anisotropic absorbing materials with surface-normal oriented optic-axis. Communication at the ICSE VI conference, Kyoto, Japan 2013.
[35] Kattner J, Hoffmann H. Simultaneous determination of thicknesses and refractive indices of ultrathin films by multiple incidence medium ellipsometry. *J. Phys. Chem. B* 2002, 106, 9723–9729.
[36] Mc Mahon JM, Schatz GC, Gray SK. Plasmonics in the ultraviolet with the poor metals Al, Ga, In, Sn, Tl, Pb and Bi. *Phys. Chem. Chem. Phys.* 2013, 15, 5415–5423.
[37] Khurgin JB, Sun G. In search of the elusive lossless metal. *Appl. Phys. Lett.* 2010, 96, 181102.
[38] Blaber MG, Arnold MD, Ford MJ. A review of the optical properties of alloys and intermetallics for plasmonics. *J. Phys. C: Cond. Mat.* 2010, 22, 143201–143227.
[39] Tripura Sundari S, Chandra S, Tyagi AK. Temperature dependent optical properties of silver from spectroscopic ellipsometry and density functional theory calculations. *J. Appl. Phys.* 2013, 114, 033515.
[40] Olmon RL, Slovick B, Johson TW, Shelton D, Oh SH, Boreman GD, Raschke MB. Optical dielectric function of gold. *Phys. Rev. B* 2012, 86, 235147.
[41] Chen KP, Drachev VP, Borneman JD, Kildishev AV, Shalaev AV. Drude relaxation rate in grained gold nanoantennas. *Nano Lett.* 2010, 10, 916–922.
[42] Park JH, Nagpal P, Oh SH, Norris DJ. Improved dielectric functions in metallic films obtained via template stripping. *Appl. Phys. Lett.* 2012, 100, 081105.
[43] Diest K, Liberman V, Lennon DM, Welander PB, Rothschild M. Aluminium plasmonics: optimization of plasmonic properties using liquid-prism-coupled ellipsometry. *Opt. Expr.* 2013, 21, 28638.

[44] Debessai M, Filip P, Aouadi SM. Niobium zirconium nitride sputter-deposited protective coatings. *Appl. Surf. Sci.* 2004, 236, 63–70.
[45] Aouadi SM, Wong KC, Mitchell KAR, Namavar F, Tobin E, Mihut DM, Rohde SL. Characterization of titanium chromium nitride nanocomposite protective coatings. *Appl. Surf. Sci.* 2004, 229, 387–394.
[46] Aouadi SM, Debessai M, Namavar F, Wong KC, Mitchell KAR. Titanium boron nitride films grown by ion beam deposition: chemical and optical characterization. *Surf. Coat. Tech.* 2004, 183, 369–377.
[47] Aouadi SM, Bohnhof A, Amriou T, Haasch RT, Williams M, Hilfiker JN. Electronic and optical properties of $Ta_{1-x}Zr_xN$ films: experimental and ab initio studies. *J. Vac. Sci. Technol.* A 2005, 23, 705.
[48] Aouadi SM, Bohnohf A, Amriou T, Williams M, Hilfiker JN, Singh N, Woollam JA. Vacuum ultra-violet spectroscopic ellipsometry study of single- and multi-phase nitride protective films. *J. Phys. Condens. Matter* 2006, 18, S1691–S1701.
[49] Tripura Sundari S, Ramaseshan R, Jose F, Dash S, Tyagi AK. Temperature dependence of dielectric constants in titanium nitride. *J. Appl. Phys.* 2014, 115, 033516.
[50] Logothetidis S, Meletis EI, Stergioudis G, Adjaottor AA. Room temperature oxidation behavior of TiN thin films. *Thin Sol. Films* 1999, 338, 304–313.
[51] Guler U, Naik GV, Boltasseva A, Shalaev VM, Kildishev AV. Performance analysis of nitride alternative plasmonic materials for localized surface plasmon applications. *Appl. Phys. B* 2012, 107, 285–291.
[52] Naik GV, Schroeder JL, Ni X, Kildishev AV, Sands TD, Boltasseva A. Titanium nitride as a plasmonic material for visible and near infrared wavelengths. *Opt. Mater. Exp.* 2012, 2, 478.
[53] Minami T. Transparent conducting oxide semiconductors for transparent electrodes. *Semicond. Sci. Technol.* 2005, 20, S35–S44.
[54] Gerfin T, Grätzel M. Optical properties of tin-indium oxide determined by spectroscopic ellipsometry. *J. Appl. Phys.* 1996, 79, 1722.
[55] Baum M, Alexeev I, Latzel M, Christiansen SH, Schmidt M. Determination of the effective refractive index of nanoparticulate ITO layers. *Opt. Exp.* 2013, 21, 22754.
[56] Rovira PI, Collins RW. Analysis of the specular and textured SnO_2:F films by high speed four-parameter Stokes vector spectroscopy. *J. Appl. Phys.* 1999, 85, 2015.
[57] Akagawa M, Fujiwara H. Optical characterization of textured SnO_2:F layers using spectroscopic ellipsometry. *J. Appl. Phys.* 2012, 112, 083507.
[58] Volintiru I, Creatore M, van de Sanden MCM. In situ spectroscopic ellipsometry growth studies on the Al-ZnO films deposited by remote plasma-enhanced metalorganic chemical vapor deposition. *J. Appl. Phys.* 2008, 103, 033704.
[59] Fujiwara H, Kondo M. Effect of carrier concentration on the dielectric function of ZnO:Ga and In_2O_3:Sn studied by spectroscopic ellipsometry: analysis of free-carrier and band-edge absorption. *Phys. Rev. B* 2005, 71, 075109.
[60] Naik GV, Kim J, Boltasseva A. Oxides and nitrides as alternative plasmonic materials in the optical range. *Opt. Mat. Exp.* 2011, 1, 1090.
[61] Sachet E, Losego MD, Guske J, Franzen S, Maria JP. Mid-infrared surface plasmon resonance in zinc oxide semiconductor thin films. *Appl. Phys. Lett.* 2013, 102, 051111.
[62] Garcia G, Buansanti llorders A, Runnerstrom, Bergerud A, Milliron DJ. Near-infrared spectrally selective plasmonic electrochromic thin films. *Adv. Opt. Mater.* 2013, 1, 215–220.
[63] Zhao Y, Pan H, Lou Y, Qiu X, Zhu J, Burda C. Plasmonic $Cu_{2-x}S$ nanocrystals: optical and structural properties of copper-deficient copper(I) sulfides. *J. Am. Chem. Soc.* 2009, 131, 4253–4261.
[64] Dorfs D, Härtling T, Miszta K, Bigall NC, Kim MR, Genovese A, Falqui A, Povia M, Manna L. Reversible tunability of the near-infrared valence band plasmon resonance in $Cu_{2-x}Se$ nanocrystals. *J. Am. Chem. Soc.* 2011, 133, 11175–11180.
[65] Zhu G, Gu L, Kitur J K, Urbas A, Vella J, Noginov MA. Organic materials with negative and controllable electric permittivity. Quantum Electronics and Laser Science Conference (QELS), OSA Technical Digest 2011 paper: QThC3.
[66] Toudert J, Serna R, Jiménez de Castro M. Exploring the optical potential of nano-bismuth: tunable surface plasmon resonances in the near ultraviolet-to-near infrared range. *J. Phys. Chem. C* 2012, 116, 20530–20539.
[67] Lautenschlager P, Garriga M, Viña L, Cardona M. Temperature dependence of the dielectric function and interband critical points in silicon. *Phys. Rev. B* 1987, 36, 4821.
[68] Logothetidis S, Polatoglou HM, Petalas, Fuchs D, Johnson RL. Investigation of the electronic transitions of cubic SiC. *Physica B* 1993, 185, 388–393.
[69] Feneberg M, Röppischer M, Cobet C, Esser N, Schörmann J, Schupp T, As DJ, Hörich F, Bläsing J, Krost A, Goldhahn R. Optical properties of GaN from 1 to 20 eV. *Phys. Rev. B* 2012, 85, 155207.
[70] Viña L, Logothetidis S, Cardona M. Temperature dependence of the dielectric function of germanium. *Phys. Rev. B* 1984, 30, 1979.
[71] Arakawa ET, Inagaki T, Williams MW. Optical properties of metals by spectroscopic ellipsometry. *Surf. Sci.* 1980, 96, 248–274.
[72] Vivekchand SRC, Engel CJ, Lubin SM, Blaber MG, Zhou W, Suh JY, Schatz GC, Odom TW. Liquid plasmonics: manipulating surface plasmon polaritons via phase transitions. *Nano Lett.* 2012, 12, 4324–4328.
[73] Dogel S, Nattland D, Freyland W. Complete wetting transitions at the liquid-vapor interface of gallium-bismuth alloys: single-wavelength and spectroscopic ellipsometry studies. *Phys. Rev. B* 2005, 72, 085403.
[74] Inagaki T, Arakawa ET, Cathers AR, Glastad KA. Optical properties of Pb and Bi between 0.6 and 3.7 eV. *Phys. Rev. B* 1982, 25, 6130–6138.
[75] Haro Poniatowski E, Serna R, Jiménez de Castro M, Súarez García A, Afonso CN, Vickridge I. Size-dependent thermo-optical properties of embedded Bi nanostructures. *Nanotechnology* 2008, 19, 485708.
[76] Nattland D, Müller SC, Poh PD, Freyland W. Wetting phenomena at the liquid-vapor interface of gallium-bismuth alloys studied by spectroscopic ellipsometry. *J. Non-Cryst. Sol.* 1996, 205–207, 772–775.
[77] Bartel K, Nattland D, Kumar A, Dogel S, Freyland W. Ellipsometric characterization of surface freezing in Ga-based alloys. *J. Phys. Cond. Matter* 2006, 18, 3535–3542.

[78] Staroske S, Freyland W, Nattland D. Tetra point wetting liquid K-KCl mixtures: spectroscopic characterization of the mesoscopic wetting and prewetting films. *J. Chem. Phys.* 2001, 115, 7669.
[79] Freyland W. Interfacial phase transitions in conducting fluids. *Phys. Chem. Chem. Phys*. 2008, 10, 923–936.
[80] Havstad MA, McLean W, Self SA. Apparatus for the measurement of the optical constants and thermal radiative properties of pure liquid metals from 0.4 to 10 um. *Rev. Sci. Instr.* 1993, 84, 1971–1978.
[81] Schmid M, Zhender S, Schwaller P, Neuenschwander B, Zürcher J, Hunziker U. Measuring the complex refractive index of metals in the solid and liquid state and its influence on the laser machining. *Proc. SPIE* 2013, 8607.
[82] Sheldon RI, Rinehart GH, Lashley JC, Van Pelt CE, Nordine PC, Krishnan S, Weber J K R. The optical properties of liquid plutonium at 632.8 nm. *J. Nucl. Mater.* 2003, 312, 207–211.
[83] Sheldon RI, Rinehart GH, Krishnan S, Nordine PC. The optical properties of liquid cerium at 632.8 nm. *Mater. Sci. Eng. B* 2001, 79, 113–122.
[84] Krishnan S, Richard Weber JK, Anderson CD, Nordine PC, Morton CT, Hofmeister H, Bayuzick RJ. Supersaturation and optical properties of metal-rich Zr-O and Zr-N liquids. *Mater. Sci. Eng.* 1996, A219, 21–25.
[85] Nagashima M, Wada H. Near infrared properties of laser ablated VO_2 thin films by ellipsometry. *Thin Sol. Films* 1998, 312, 61–65.
[86] Nazari M, Zhao Y, Kuryatkov VV, Fan ZY, Bernussi AA, Holtz M. Temperature dependence of the optical properties of VO_2 deposited on sapphire with different orientations. *Phys. Rev. B* 2013, 87, 035142.
[87] Ishiwata Y, Suehiro S, Kida T, Ishii H, Tezuka Y, Osato H, Watanabe E, Tsuya D, Inagaki Y, Kawae T, Nantoh M, Ishibaki K. Spontaneous uniaxial strain and disappearance of the metal-insulator transition in monodisperse V_2O_3 nanocrystals. *Phys. Rev. B* 2012, 86, 035449.
[88] Qazilbash MM, Schafgans AA, Burch KS, Yun SJ, Chae BG, Kim BJ, Kim HT, Basov DN. Electrodynamics of the vanadium oxides VO_2 and V_2O_3. *Phys. Rev. B* 2008, 77, 115121.
[89] Stewart MK, Brownstead D, Wang S, West KG, Ramirez JG, Qazilbash MM, Perkins NB, Schuller IK, Basov BN. Insulator-to-metal transition and correlated metallic state of V_2O_3 investigated by optical spectroscopy. *Phys. Rev. B* 2012, 85, 205113.
[90] Lopez R, Haynes TE, Boatner LA, Feldman LC, Haglund Jr RF. Temperature-controlled surface plasmon resonance in VO_2 nanorods. *Opt. Lett.* 2002, 27, 1327.
[91] Rini M, Cavalleri A, Schoenlein RW, López R, Feldman LC, Haglund Jr RF, Boatner LA, Haynes TE. Photoinduced phase transition in VO_2 nanocrystals: ultrafast control of surface plasmon resonance. *Opt. Lett.* 2005, 30, 558.
[92] Li S Y, Niklasson GA, Granqvist CG. Nanothermochromics: calculations for VO_2 nanoparticles in dielectric hosts show much improved luminous transmittance and solar energy transmittance modulation. *J. Appl. Phys.* 2010, 108, 063525.
[93] Ferrara DW, Nag J, MacQuarrie ER, Kaye AB, Haglund Jr RF. Plasmonic probe of the semiconductor to metal phase transition vanadium dioxide. *Nano Lett.* 2013, 13, 4169.
[94] Shportko K, Kremers S, Woda M, Lencer D, Robertson J, Wuttig M. Resonant bonding in crystalline phase-change materials. *Nat. Mater.* 2008, 7, 653.
[95] Wei SJ, Zhu HF, Chen K, Xu D, Li J, Gan FX, Zhang Y, Xia YJ, Li GH. Phase change behavior in titanium-doped $Ge_2Sb_2Te_5$ films. *Appl. Phys. Lett.* 2011, 98, 231910.
[96] Wei S J, Li J, Wu X, Zhou P, Wang S, Zheng Y, Chen L, Gan F, Zhang X, Li G. Phase change characteristics of aluminium doped $Ge_2Sb_2Te_5$ films prepared by magnetron sputtering. *Opt. Exp.* 2007, 15, 10584.
[97] Wang K, Wamwangi D, Ziegler S, Steimer C, Wuttig M. Influence of Bi doping upon the phased change characteristics of $Ge_2Sb_2Te_5$. *J. Appl. Phys.* 2004, 96, 5557.
[98] Kuwahara M, Endo R, Tsutsumi K, Morkosa F, Tsuruoka T, Fukaya T, Suzuki M, Susa M, Endo T, Tadokoro T. Approach for measuring complex refractive index of molten Sb_2T_3 by spectroscopic ellipsometry. *Appl. Phys. Lett.* 2012, 100, 101910.
[99] Drevillon B. Spectroscopic ellipsometry of ultrathin films: from UV to IR. *Thin Sol. Films* 1988, 163, 157–166.
[100] Antoine AM, Drevillon B. In-situ investigation of the early stage of the growth of a-Si:H on silica and tin dioxide substrates. *J. Non-Cryst. Sol.* 1987, 97–98, 1403–1406.
[101] Marsillac S, Collins RW. Spectroscopic ellipsometry: metrology for photovoltaics from the nanoscale to gigawatts. *Proc. SPIE* 2012, 8256, 825613.
[102] Oates TWH, Ryves L, Bilek MMM. Dynamic spectroscopic ellipsometry determination of nanostructural changes in plasmonic silver films. *Opt. Exp.* 2007, 15, 15987.
[103] Fujiwara H, Kondo M, Matsuda A. Real-time spectroscopic ellipsometry studies of the nucleation and grain growth processes in microscrystalline silicon thin films. *Phys. Rev. B* 2001, 63, 115306.
[104] Hövel M, Gompf B, Dressel M. Dielectric properties of ultrathin metal films around the percolation threshold. *Phys. Rev. B* 2010, 81, 035402.
[105] Oates TWH, McKenzie DR, Bilek MMM. Percolation threshold in ultrathin titanium thin films determined by in situ spectroscopic ellipsometry. *Phys. Rev. B* 2004, 70, 195406.
[106] Little SA, Begou T, Collins RW, Marsillac S. Optical detection of melting point depression for silver nanoparticles via in situ real time spectroscopic ellipsometry. *Appl. Phys. Lett.* 2012, 100, 051107.
[107] Wu PC, Losurdo M, Kim TH, Giangregorio M, Bruno G, Everitt HO, Brown AS. Plasmonic gallium nanoparticles on polar semiconductors: interplay between nanoparticle wetting, localized surface plasmon dynamics, and interface charge. *Langmuir* 2009, 25, 924–930.
[108] Wu PC, Kim TH, Suvorova A, Giangregorio M, Saunders M, Bruno G, Brown AS, Losurdo M. GaMg alloy nanoparticles for broadly tunable plasmonics. *Small* 2011, 7, 751–756.
[109] Yi C, Kim TH, Jiao W, Yang Y, Lazarides A, Hingerl K, Bruno G, Brown A, Losurdo M. Evidence of plasmonic coupling in gallium nanoparticles/graphene/SiC. *Small* 2012, 8, 2721–2730.
[110] Wu PC, Kim TH, Brown AS, Losurdo M, Bruno G, Everitt HO. Real-time resonance tuning of liquid Ga nanoparticles by in situ spectroscopic ellipsometry. *Appl. Phys. Lett.* 2007, 90, 103119.
[111] Wu PC, Losurdo M, Kim TH, Garcia-Cueto B, Moreno F, Bruno G, Brown AS. Ga-Mg core-shell nanosystem for a novel full color plasmonics. *J. Phys. Chem. C* 2011, 115, 13571–13576.

[112] Koh J, Lu Y. Wronski CR, Kuang Y, Collins RW, Tsong TT, Strausser Y E. Correlation of real time spectroellipsometry and atomic force microscopy measurements of surface roughness on amorphous semiconductor thin films. *Appl. Phys. Lett.* 1996, 69, 1297.
[113] Uhrenfeld C, Chevallier J, Larsen AN, Nielsen BB. Near-infrared-ultraviolet absorption cross sections for Ge nanocrystals in SiO_2 thin films: effects of shape and layer structure. *J. Appl. Phys.* 2011, 109, 094314.
[114] Bulutay C. Interband, intraband, and excited-state direct photon absorption of silicon and germanium nanocrystals embedded in a wide band-gap lattice. *Phys. Rev. B* 2007, 76, 205321.
[115] Amans D, Callard S, Gagnaire A, Joseph J, Ledoux G, Huisken F. Ellipsometric study of silicon nanocrystal optical constants. *J. Appl. Phys.* 2003, 93, 4173.
[116] Gallas B, Stenger I, Kao CC, Fisson S, Vuye G, Rivory J. Optical properties of Si nanocrystals embedded in SiO_2. *Phys. Rev. B* 2005, 72, 155319.
[117] Mansour M, En Naciri A, Johann L, Grob JJ, Stchakovsky M. Dielectric function and optical transitions of silicon nanocrystals between 0.6 eV and 6.5 eV. *Phys. Stat. Sol. (a)* 2008, 205, 845–848.
[118] Fujiwara H, Koh J, Collins RW. Assessment of effective-medium theories in the analysis of nucleation and microscopic surface roughness evolution for semiconductor thin films. *Phys. Rev. B* 2000, 61, 10832.
[119] Moreno JA, Garrido B, Pellegrino P, Garcia C, Arbiol J, Morante JR, Marie P, Gourbilleau F, Rizk R. Size dependence of refractive index of Si nanoclusters embedded in SiO_2. *J. Appl. Phys.* 2005, 98, 013523.
[120] Ding L, Chen TP, Liu Y, Yang M, Wong JI, Liu YC, Trigg DA, Zhu FR, Tan MC, Fung S. Influence of nanocrystal size on optical properties of Si nanocrystals embedded in SiO_2 synthesized by Si ion implantation. *J. Appl. Phys.* 2007, 101, 103525.
[121] Chen TP, Liu Y, Tse MS, Tan OK, Ho PF, Liu KY, Gui D, Tan ALK. Dielectric functions of Si nanocrystals embedded in SiO_2 matrix. *Phys. Rev. B* 2003, 68, 153301.
[122] Ding L, Chen TP, Wong JI, Yang M, Liu Y, Ng CY, Liu Y C, Tung CH, Trigg AD, Fung S. Dielectric functions of densely stacked Si nanocrystal layer embedded in SiO_2 thin films. *Appl. Phys. Lett.* 2006, 89, 251910.
[123] Alonso MI, Marcus IC, Garriga M, Goñi AR, Jedrzejewski J, Balberg I. Evidence of quantum confinements effects on interband optical transitions in Si nanocrystals. *Phys. Rev. B* 2010, 82, 045302.
[124] Losurdo M, Giangregorio MM, Capezzuto P, Bruno G, Cerquera MF, Alves E, Stepikhova M. Dielectric function of nanocrystalline silicon with few nanometers (<3 nm) grain size. *Appl. Phys. Lett.* 2003, 82, 2993.
[125] Keita AS, En Naciri AS, Delachat F, Carrada M, Ferblantier G, Slaoui A. Dielectric function of Si nanoparticles within a silicon nitride matrix. *Phys. Stat. Sol. C* 2010, 7, 418–422.
[126] Zhang RJ, Chen YM, lu WJ, Cai QY, Zheng YX, Chen LY. Influence of nanocrystal size on dielectric functions of Si nanocrystals embedded in SiO_2 matrix. *Appl. Phys. Lett.* 2009, 95, 161109.
[127] Stenger I, Gallas B, Siozade l, Kao CC, Chenot S, Fisson S, Vuye G, Rivory J. Evolution of the optical properties of Si nanoparticles embedded in SiO_2 as function of annealing conditions. *J. Appl. Phys.* 2008, 103, 114303.
[128] Keita AS, En Naciri A, Delachat F, Carrada M, Ferblantier G, Slaoui A. Ellipsometric demonstration of the existence of a strong correlation between size distribution and optical response of silicon nanoclusters in a nitride matrix. *Appl. Phys. Lett.* 2011, 99, 131903.
[129] Keita AS, En Naciri A. Size distribution dependence of the dielectric function of Si quantum dots described by a modified Maxwell-Garnett formulation. *Phys. Rev. B* 2011, 84, 12436.
[130] En Naciri A, Miska P, Keita AS, Battie Y, Rinnert H, Vergnat M. Optical properties of uniformly sized silicon nanocrystals within a single silicon oxide layer. *J. Nanopart. Res.* 2013, 15, 1538.
[131] Kreibig U, Vollmer M. *Optical properties of metal clusters*, Springer-Verlag: Berlin Heidelberg, 1995.
[132] Peng S, McMahon JM, Schatz GC, Gray SK, Sun Y. Reversing the size-dependence of surface plasmon resonances. *PNAS* 2013, 110, 4212.
[133] Drachev VP, Chettiar UK, Kildishev AV, Yuan HK, Cai W, Shalaev VM. The Ag dielectric function in plasmonic metamaterials. *Opt. Exp.* 2008, 16, 1186.
[134] Losurdo M, Giangregorio MM, Bianco GV, Suvorova AA, Kong C, Rubanoc S, Capezzuto P, Humlicek J, Bruno G. Size dependence of the dielectric function of silicon-supported plasmonic gold nanoparticles. *Phys. Rev. B* 2010, 82, 155451.
[135] Nguyen HV, An I, Collins RW. Evolution of the optical functions of thin-film aluminium: a real-time spectroscopic ellipsometry study. *Phys. Rev. B* 1993, 47, 3947.
[136] Anno E, Tanimoto M. Size-dependent change in parallel band absorption of Al particles. *Phys. Rev. B* 2001, 64, 165407.
[137] Hägglund C, Zeltzer G, Ruiz R, Thomann I, Lee HBR, Brongersma ML, Bent SF. Self-assembly based plasmonic arrays tuned by atomic layer deposition for extreme visible light absorption. *Nano Lett.* 2013, 13, 3352–3357.
[138] Sánchez Valencia JR, Toudert J, Borras A, Barranco A, Lahoz R, De la Fuente GF, Frutos F, Gonzalez Elipe AR. Selective dichroic patterning by nanosecond laser treatment of Ag nanostripes. *Adv. Mater.* 2011, 23, 248.
[139] Liu Y, Zhang X. Metamaterials: a new frontier of science and technology. *Chem. Soc. Rev.* 2011, 40, 2494–2507.
[140] Toudert J, Babonneau D, Simonot L, Camelio S, Girardeau T. Quantitative modelling of the surface plasmon resonances of metal nanoclusters sandwiched between dielectric layers: the influence of nanocluster size, shape and organization. *Nanotechnology* 2008, 19, 125709.
[141] Mendoza-Galván A, Järrendahl K, Dmitriev A, Pakizeh T, Käll M. Arwin A. Optical response of supported gold nanodisks. *Opt. Exp.* 2011, 19, 12093.
[142] Mendoza-Galván A, Järrendahl K, Dmitriev A, Pakizeh T, Käll M, Arwin H. Fano interference in supported nanosandwiches with weakly coupled nanodisks. *Opt. Exp.* 2012, 20, 29646.
[143] Pakizeh T, Dmitriev A, Abrishamian MS, Granpayeh N, Käll M. Structural asymmetry and induced optical magnetism in plasmonic nanosandwiches. *J. Opt. Soc. Am. B* 2008, 25, 659.
[144] Verre R, Fleischer K, Smith C, McAlinden N, McGilp JF, Shvets IV. Probing the out-of-plane optical response of plasmonic nanostructures using spectroscopic ellipsometry. *Phys. Rev. B* 2011, 84, 085440.
[145] Verre R, Modreanu M, Ualibek O, Fox D, Fleischer K, Smith C Zhang H, Pemble M, McGilp JF, Shvets I V. General approach to the analysis of plasmonic structures using spectroscopic ellipsometry. *Phys. Rev. B* 2013, 87, 235428.

[146] Oates TWH, Ranjan M, Facsko S, Arwin H. Highly anisotropic effective dielectric functions of silver nanoparticle arrays. *Opt. Exp.* 2011, 19, 2014.
[147] Jen YJ, Lakhtakia A, Yu CW, Lin CT. Vapor-deposited thin films with negative real refractive index in the visible regime. *Opt. Exp.* 2009, 17, 7784.
[148] Beydaghyan G, Buzea C, Cui Y, Elliott C, Robbie K. Ex situ ellipsometric investigation of nanocolumns inclination angle of obliquely evaporated silicon thin films. *Appl. Phys. Lett.* 2005, 87, 153103.
[149] Schmidt D, Booso B, Hofmann T, Schubert E, Sarangan A, Schubert M. Generalized ellipsometry for monoclinic absorbing materials: determination of optical constants of Cr columnar thin films. *Opt. Lett.* 2009, 34, 992.
[150] Schmidt D, Booso B, Hofmann T, Schubert E, Sarangan A, Schubert M. Monoclinic optical constants, birefringence, and dichroism of slanted titanium nanocolumns determined by generalized ellipsometry. *Appl. Phys. Lett.* 2009, 94, 011914.
[151] Schmidt D, Schubert E, Schubert M. Optical properties of cobalt slanted columnar thin films passivated by atomic layer deposition. *Appl. Phys. Lett.* 2012, 100, 011912.
[152] Schmidt D, Schubert M. Anisotropic Bruggeman effective medium approaches for slanted columnar thin films. *J. Appl. Phys.* 2013, 114, 083510.
[153] Kasputis T, Koenig M, Schmidt D, Sekora D, Rodenhausen KB, Eichorn KJ, Uhlmann P, Schubert E, Pannier AK, Schubert M, Stamm M. Slanted columnar thin films prepared by glancing angle deposition functionalized with polyacrylic acid polymer brushes. *J. Phys. Chem. C* 2013, 117, 13971–13980.
[154] Liang D, Schmidt D, Wang H, Schubert E, Schubert M. Generalized ellipsometry effective medium approximation analysis approach of porous slanted columnar thin films infiltrated with polymer. *Appl. Phys. Lett.* 2013, 103, 111906.
[155] May RA, Flaherty DW, Mullins CB, Stevenson KJ. Hybrid generalized ellipsometry and quartz crystal microbalance nanogravimetry for the detection of adsorption isotherms on biaxial metal oxide films. *J. Phys. Chem. Lett.* 2010, 1, 1264–1268.
[156] Hofmann T, Schmidt D, Boosalis A, Kühne P, Skomski R, Herzinger CM, Woollam, Schubert M, Schubert E. THz dielectric anisotropy of metal slanted colunar thin films. *Appl. Phys. Lett.* 2011, 99, 081903.
[157] Schmidt D, Müller C, Hofmann T, Inganäs O, Arwin H, Schubert E, Schubert M. Optical properties of hybrid titanium chevron sculptured thin films coated with a semiconducting polymer. *Thin Sol. Films* 2011, 519, 2645–2649.
[158] Gallas B, Robbie K, Abdeddaïm, Guida G, Yang J, Rivory J, Priou A. Silver square nanospirals mimic optical properties of U-shaped metamaterials. *Opt. Exp.* 2010, 18, 16335.
[159] Oates TWH, Dastmalchi B, Isic G, Tollabimazraehno S, Helgert C, Pertsch T, Kley EB, Verschuuren MA, Bergmair I, Hingerl K, Ninrichs K. Oblique incidence ellipsometric characterization and the substrate dependence of visible frequency fishnet metamaterials. *Opt. Exp.* 2012, 20, 11166.
[160] Menzel C, Rockstuhl C, Paul, T, Lederer F, Pertsch T. Retrieving effective parameters for metamaterials at oblique incidence. *Phys. Rev. B* 2008, 77, 195328.
[161] Menzel C, Paul T, Rockstuhl C, Pertsch T, Tretyakov S, Lederer F. Validity of effective material parameters for optical fishnet metamaterials. *Phys. Rev. B* 2010, 81, 035320.
[162] Gompf B, Braun J, Weiss T, Giessen H, Dressel M. Periodic nanostructures: spatial dispersion mimics chirality. *Phys. Rev. Lett.* 2011, 106, 185501.
[163] Jakovljevic, Isic G, Vasic B, Oates T W H, Hinrichs K, Bergmair I, Hingerl K, Gajic R. Spectroscopic ellipsometry of split ring resonators at infrared frequencies. *Appl. Phys. Lett.* 2012, 100, 161105.
[164] Guth N, Gallas B, Rivory J, Grand J, Ourir A, Guida G, Abdeddaim R, Jouvaud C, de Rosny J. Optical properties of metamaterials: influence of electric multipoles, magneto-electric coupling, and spatial dispersion. *Phys: Rev. B* 2012, 85, 115138.
[165] Malassis L, Massé P, Tréguer-Delapierre M, Mornet S, Weisbecker P, Kravets V, Grigorenko A, Barois P. Bottom-up fabrication and optical characterization of dense films of metal-atoms made of core-shell plasmonic nanoparticles. *Langmuir* 2013, 29, 1551–1561.
[166] Dintinger J, Mühlig S, Rockstuhl C, Scharf T. A bottom-up approach to fabricate optical metamaterials by self-assembled metallic nanoparticles. *Opt. Mater. Exp.* 2012, 2, 269.
[167] Hoffman AJ, Alekseyev L, Howard SS, franz KJ, Wasserman D, Podolskiy VA, Narimanov EE, Sivco DL, Gmachl C. Negative refraction in semiconductor metamaterials. *Nat. Mater.* 2007, 6, 946.
[168] Naik GV, Liu J, Kildishev AV, Shalaev VM, Boltasseva A. Demonstration of Al:ZnO as a plasmonic component for near-infrared metamaterials. *PNAS* 2012, 109, 8834–8838.
[169] Arwin H. Is ellipsometry suitable for sensor applications? *Sens. Act. A* 2001, 92, 43.
[170] Nooke A, Beck U, Hertwig A, Krause A, Krüger H, Lohse V, Negendank D, Steinbach J. Ellipsometric detection of gases with the surface plasmon resonance effect on gold top-coated with sensitive layers. *Thin Sol. Films* 2011, 519, 2659–2663.
[171] Lodewijks K, Van Roy W, Borghs G, Lagae L, Van Dorpe P. Boosting the figure-of-merit of LSPR-based refractive index sensing by phase-sensitive measurements. *Nano Lett.* 2012, 12, 1655–1659.
[172] Chen S, Li G, Wong W, Pun EYB, Cheah KW. Sharp plasmonic resonance on gold gratings in amplitude and phase domains. *Appl. Opt.* 2012, 51, 8563.
[173] Kravets VG, Schedin F, Kabashin AV, Grigorenko AN. Sensitivity of collective plasmon modes of gold nanoresonators to local environment. *Opt. Lett.* 2010, 35, 956.
[174] Kravets VG, Schedin F, Jalil R, Britnell L, Gorbachev RV, Ansell D, Thackray, Novoselov KS, Geim AK, Kabashin AV, Grigorenko AN. Singular phase nano-optics in plasmonic metamaterials for label-free single-molecule detection. *Nat. Mater.* 2013, 12, 304.
[175] Malassis L, Massé P, Tréguer-Delapierre M, Mornet S, Weisbecker P, Barois P, Simovski CR, Kravets VG, Grigorenko AN. Topological darkness in self-assembled plasmonic metamaterials. *Adv. Mater.* 2013, 26, 324.
[176] Aas LMS, Kildemo M, Cohin Y, Sondergard E. Determination of small tilt angles of short GaSb nanopillars using UV-visible Mueller matrix ellipsometry. *Thin Sol. Films* 2013, 541, 97–101.
[177] Foldyna M, Germer TA, Bergner BC, Dixson RG. Generalized ellipsometry of artificially designed line width roughness. *Thin Sol. Films* 2011, 519, 2633–2636.

[178] Patrick HJ, Germer TA, Ding Y, Ro HW, Richter LJ, Soles CL. In situ measurement of annealing-induced line shape evolution in nanoimprinted polymers using scatterometry. *Proc. SPIE* 2009, 7271, 727128.
[179] Stabo-Eeg F, Kildemo M, Nerbo IS, Lindgren M. Well-conditioned multiple laser Mueller matrix ellipsometer. *Opt. Eng.* 2008, 47, 073604.
[180] Hoydalsvik K, Aas LMS, Doli E, Sondergard E, Kildemo M, Breiby DW. Combining surface X-ray scattering and ellipsometry for non-destructive characterization of ion-beam induced GaSb surface nanostructures. *Thin Sol. Films*, 2013, in press. Available online 29 October 2013.
[181] Cheung KT, Foo Y, To CH, Zapien JA. Towards FDTD modeling of spectroscopic ellipsometry data at large angles of incidence. *Appl. Surf. Sci.* 2013, 281, 2–7.

Johann Toudert is a postdoctoral associate in the Laser Processing Group of the Instituto de Óptica – CSIC, Madrid (Spain). In 2005, he received his PhD degree, together with an outstanding PhD award, from the Poitiers University, France. After postdoctoral stays at the Instituto de Óptica, at the Troyes University (France), and at the Institute of Materials Science of Seville – CSIC (Spain), he obtained two excellence postdoctoral fellowship grants – from the CSIC (JAE fellowship programme) and the Spanish Ministry for Science and Innovation (Juan de la Cierva fellowship programme). His scientific interests are related to the development of multiscale active optical materials, plasmonics, nanofabrication, optical spectroscopy and modeling, photonic applications.